Contrib Mineral Petrol (2013) 166:329–349
DOI 10.1007/s00410-013-0878-1

ORIGINAL PAPER

Experiments on liquid immiscibility in silicate melts with H_2O, P, S, F and Cl: implications for natural magmas

G. W. Lester · A. H. Clark · T. K. Kyser · H. R. Naslund

Received: 7 July 2011 / Accepted: 9 April 2013 / Published online: 16 May 2013
© Springer-Verlag Berlin Heidelberg 2013

Abstract Isobaric (200 MPa) experiments have been performed to investigate the effects of H_2O alone or in combination with P, S, F or Cl on liquid-phase separation in melts in the systems Fe_2SiO_4–Fe_3O_4–$KAlSi_2O_6$–SiO_2, Fe_3O_4–$KAlSi_2O_6$–SiO_2 and Fe_3O_4–Fe_2O_3–$KAlSi_2O_6$–SiO_2 with or without plagioclase (An_{50}). Experiments were heated in a rapid-quench internally heated pressure vessel at 1,075, 1,150 or 1,200 °C for 2 h. Experimental fO_2 was maintained at QFM, NNO or MH oxygen buffers. H_2O alone or in combination with P, S or F increases the temperature and composition range of two-liquid fields at fO_2 = NNO and MH buffers. P, S, F and Cl partition preferentially into the Fe-rich immiscible liquid. Two-liquid partition coefficients for Fe, Si, P and S correlate well with the degree of polymerization of the SiO_2-rich liquid and plot on similar but distinct power-law curves compared with equivalent anhydrous or basaltic melts. The addition of 2 wt% S to the system Fe_3O_4–Fe_2O_3–$KAlSi_2O_6$–SiO_2 stabilizes three immiscible melts with Fe-, FeS- and Si-rich compositions. H_2O-induced suppression of liquidus temperatures in the experimental systems, considered with the effects of pressure on the temperature and composition ranges of two-liquid fields in silicate melts, suggests that liquid-phase separation may be stable in some H_2O-rich silicate magmas at pressures in excess of 200 MPa.

Keywords Immiscible oxide melts · Immiscible magma · Two-liquid partitioning · Immiscible

Communicated by G. Moore.

G. W. Lester (✉) · A. H. Clark · T. K. Kyser
Department of Geological Sciences and Geological Engineering, Miller Hall, Queens University, 99 University Avenue, Kingston, ON K7L 3N6, Canada
e-mail: glesfo2@yahoo.com

H. R. Naslund
Department of Geological Sciences and Environmental Studies, Binghamton University, PO BOX 6000, Binghamton, NY 13902-6000, USA

Introduction

Liquid-phase separation is accepted as an important differentiation mechanism in diverse magmas. Immiscibility between felsic silicate-dominated and Fe-rich mafic silicate-dominated liquids (L^f and L^m) has been documented in layered mafic intrusions (McBirney 1975), anorthosite complexes (Darling and Florence 1995), mid-ocean ridge magma chambers (Dixon and Rutherford 1979), granitoids (Rajesh 2003; Johnson et al. 2002), lamprophyres (Philpotts 1967) and lunar and terrestrial volcanic rocks (Roedder and Weiblen 1971). Immiscibility also has been invoked as a primary genetic mechanism for some iron oxide-dominated base and precious metal mineral deposits, including Kiruna-type magnetite–apatite systems (Chen et al. 2010, Clark and Kontak 2004, Nyström and Henríquez 1994).

Experimental investigations of felsic silicate–mafic silicate liquid immiscibility to date have constrained the configuration of miscibility gaps in silicate melts as a function of temperature, parental melt composition and, to a lesser extent, pressure for the anhydrous systems Fe_2SiO_4–$KAlSi_2O_6$–SiO_2 with or without one or more of the following: Na, Ca, Mg, Ti or P (Roedder 1951, 1978; Watson 1976a, b, Visser and Koster van Groos 1979a, b; Naslund 1983; Bogaerts and Schmidt 2006), as well as for more chemically complex lunar and terrestrial basaltic

liquids (Longhi 1990; Philpotts 1982; Hess et al. 1975; Rutherford et al. 1974). To develop further a predictive model of felsic silicate–mafic silicate immiscibility in magmas, we herein document experiments on the effects of the network-modifying component H_2O, alone and in combination with P, S, F or Cl, on selected compositions in the systems Fe_2SiO_4–Fe_3O_4–$KAlSi_2O_6$–SiO_2–Fe_3O_4–Fe_2O_3–$KAlSi_2O_6$–SiO_2, Fe_3O_4–$KAlSi_2O_6$–SiO_2, Fe_3O_4–Fe_2O_3–$KAlSi_2O_6$–SiO_2 and Fe_3O_4–Fe_2O_3–$KAlSi_2O_6$–SiO_2–$Ca_{0.5}Na_{.5}Al_{1.5}Si_{2.5}O_8$ (An_{50}).

The stability and extent of two-liquid solvi in silicate melts are markedly sensitive to minor variations in the enthalpy of mixing term in the expression: $\Delta G_{mix} = \Delta H_{mix} - T\Delta S_{mix}$. Common constituents in natural melts such as OH, P, S, F and Cl have positive enthalpies of formation of anion–metal complexes which act to increase the value of the ΔG_{mix} term, thus favoring liquid unmixing (Ryerson and Hess 1978). Further, it has been demonstrated that OH, P, S, F and Cl influence liquid miscibility gap relations and the degree of polymerization in silicate melts, parameters that control the compositions and thermal ranges of two-liquid miscibility gaps (Botcharnikov 2008; Moore et al. 1998; Visser and Koster van Groos 1979a; Haughton et al. 1974; Dolejš and Baker 2007; Webster and De Vivo 2002).

The results reported herein show that H_2O, alone or in combination with P, S, F or Cl, acts to expand the composition range of experimental two-liquid miscibility gaps at temperatures that are geologically relevant (1,075–1,200 °C). The phase relationships we document, considered in conjunction with known chemical-thermal evolution trends in natural melts, provide a more complete framework for the discussion of the role of silicate-liquid immiscibility in petrogenesis and mass–flux in natural igneous systems.

Experimental method

Starting materials for the experiments included seven anhydrous base compositions prepared from SiO_2 (cristobalite), Al_2O_3, $K_2Si_2O_5$, FeO and Fe_2O_3. Each base mixture plots as a composition point on the 30 wt% FeO isopleth on the ternary join fayalite–leucite–silica (Fig. 1). Base compositions have an Al/K molar ratio of 1. To minimize the fO_2 gradient between melts and external solid buffers, Fe^{3+}/Σ Fe values for the melts synthesized in this study were estimated with the method of Schuessler et al. (2008) at: fO_2 = quartz–fayalite–magnetite (QFM), nickel–nickel oxide (NNO) or magnetite-hematite (MH) buffers and $T = 1{,}200$ °C and P = 200 MPa. The 30 wt% FeO_{total} component of each base mixture comprises FeO and Fe_2O_3, and Fe_2P, FeS, $FeCl_2$ or FeF_2 in proportions that approximate the Fe^{3+}/Σ Fe values calculated for the selected experimental conditions. Oxygen fugacity in the experimental capsules was controlled using the conventional double capsule, metal–metal oxide or metal oxide-silicate + water configuration (Chou and Cygan 1990).

Experimental starting compositions containing either 1 wt% P, 2 wt% S, 6 wt% Cl or 6 wt% F (total wt. oxides) were prepared by the addition of Fe_2P, FeS, $FeCl_2$ or FeF_2 to the anhydrous base mixtures (Table 1). Fe salts were selected as the source of P, S, F and Cl in order to minimize the loss of volatile components during the welding of experimental capsules. Hydrous experiments incorporated 10 wt% H_2O (total wt. solids). Plagioclase-bearing experiments contain 1.3 wt% (total weight of solid oxides and halides) An_{50}, constituting 43 wt% of the feldspar component.

Experiments were carried out by loading the desired quantity of starting material, or starting material $+H_2O$, into a 2-mm-outside diameter, 1.25-cm-length, 0.1-mm-thick platinum capsule. Three to five experimental capsules were loaded into a 5-mm-outside diameter, 3-cm-length, 0.2-mm-thick platinum capsule containing H_2O and one of the selected metal–metal oxide or metal oxide–silicate buffers, QFM, NNO or MH. Both inner experimental capsules and outer buffer-bearing capsules were sealed by welding.

Experiments were carried out in Kanthal™ or platinum-wound furnaces placed in an internally heated pressure vessel under isobaric conditions (200 ± 10 MPa), isothermally at 1,075, 1,150 or 1,200 °C for two hours using argon as the pressure medium. The pressure vessel, similar in design to that described by Holloway (1971), was modified to allow the vessel to rotate from the horizontal run position to a vertical quench position. Rapid isobaric cooling of the experimental capsules was achieved as the vessel was rotated toward the vertical causing the capsule to drop from the hot spot to the unheated, water-cooled end of the pressure chamber ($T < 250$ °C). The quench rate is inferred to be 500 °C/s, similar to that reported by Holloway (1992) for a rapid-quench furnace with an equivalent thermal profile. The rotating furnace design used in this study provides a significant degree of control over the thermal characteristics of the critical heating zone. The temperature along with the length of the experimental capsules was measured using three inconel-sheathed, chrome-alumel thermocouples. Temperature differences between the distal thermocouples ranged from 1 to 16, ±2 °C. The argon medium pressure was measured using a Bourdon tube gauge, accurate to ±5 MPa.

Reversal experiments were performed to determine the time required to achieve chemical equilibrium in the experimental charges. Capsules (buffered at fO_2 = QFM, NNO and MH) containing experimental base compositions +10 wt% H_2O (total weight of solids in charge) were heated for 2 h at a temperature of 1,210 °C and then cooled

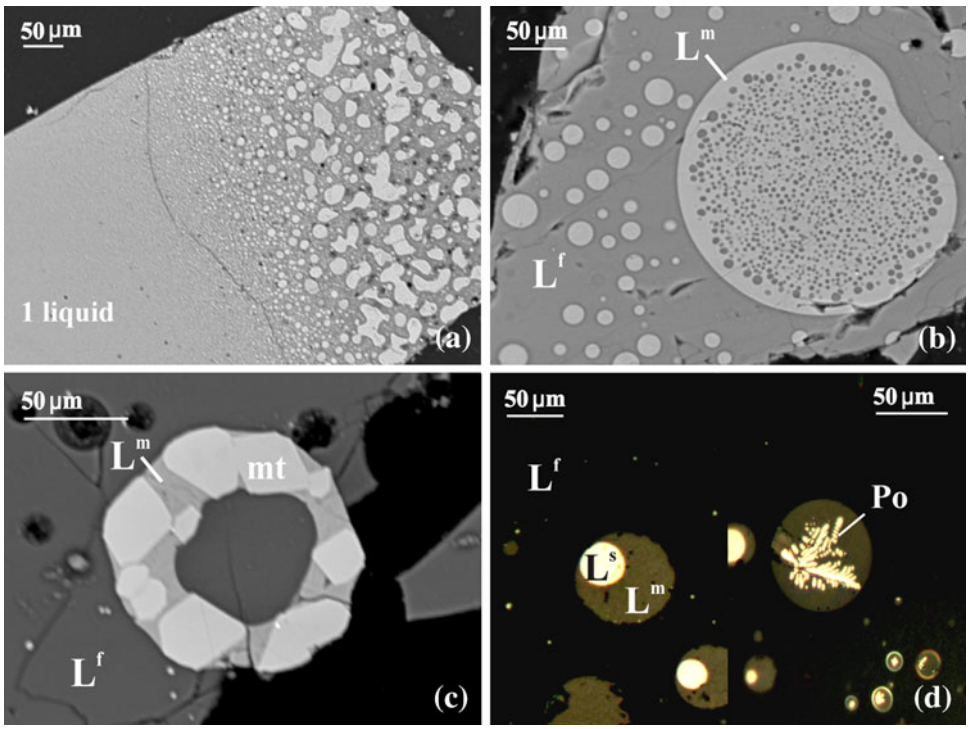

Fig. 1 Backscattered electron images of run product, **a** liquid-phase separation and coalescence of liquid droplets (L^m), composition: A-3 + H_2O + F, fO_2 = MH, P = 200 MPa, phase assemblage is the result of a thermal gradient, range ~ 950–1,230 °C (from *left* to *right*), **b** typical liquid-phase separation textures, composition: A-1 + H_2O + P, fO_2 = MH, 1,200 °C, P = 200 MPa, **c** two liquids plus magnetite, composition: A-3 + H_2O + F, fO_2 = MH, 1,075 °C, P = 200 MPa, **d** three-liquid-phase assemblage (L^f, L^m and L^s) and three liquids plus pyrrhotite (Po) developed upon cooling, A-3 + H_2O + S, fO_2 = MH, 1,150 °C, P = 200 MPa. L^f = Si-rich liquid, L^m = Fe-rich liquid, L^s = sulfide-rich liquid, Po = pyrrhotite, mt = magnetite

Table 1 Base compositions (wt%)

Base composition	SiO_2	FeO total	Al_2O_3	K_2O	An_{50}^a
A-1	66.05	30	2.06	1.89	–
A-2	64.46	30	2.88	2.66	–
A-3	62.86	30	3.71	3.43	–
A-4	60.13	30	5.13	4.74	–
A-5	57.48	30	6.51	6.01	–
A-6	55.88	30	7.34	6.78	–
A-7	54.32	30	8.15	7.53	–
An_{50}	65.2	29.62	2.03	1.87	1.3

[a] $(Ca_{0.5}\ Na_{.5})\ Al_{1.5}\ Si_{2.5}O_8$

to 1,075, 1,150 or 1,200 °C for one, two or 4 h, respectively, and subsequently quenched. The chemical compositions and textural characteristics observed in the experimental products produced in the reverse experiments are identical to those produced in forward experiments run at the same temperature, and it is concluded that equilibrium was obtained at run durations of less than 1 h. Solid-oxide buffer reactants were evaluated after cooling using X-ray powder diffraction analysis or microscopic phase identification.

Experimental samples were mounted in epoxy, polished and analyzed with a Cameca SX-100 electron microprobe at the University of Manitoba. Analytical conditions were set to an accelerating voltage of 15 kV, a 15 nA beam current and counting time of 20 s for all elements except P, S, F and Cl (30 s). The beam diameters were 5–10 µm for Si-rich and Fe-rich glasses and 2 um for quenched sulfide melt. Natural and synthetic oxides, silicates or sulfides were used as standards.

Results

General

Compositions of the starting materials are given in Table 1, run conditions and phase relation data are summarized in Table 2, and electron microprobe analyses and mass concentration partition ratios (D_i = concentration in the mafic liquid L^m/concentration in the felsic liquid L^f) are presented in Table 3.

Immiscible liquids in experimental anhydrous silicate melts commonly occur as spheroidal or ellipsoidal droplets that range from submicron to over 500 µm in size (Fig. 1).

Table 2 Experimental run conditions and phase assemblages

Base	Composition					t (°C)	Buffer	Phase assemblage	Base	Composition					t (°C)	Buffer	Phase assemblage
	Additional components (wt% base)									Additional components (wt% base)							
	H_2O	P	S	F	Cl					H_2O	P	S	F	Cl			
A-1	10	–	–	–	–	1,200	MH	2 liq.	A-2	10	1	–	–	–	1,075	NNO	2 liq.
A-2	10	–	–	–	–	1,200	MH	2 liq.	A-3	10	1	–	–	–	1,075	NNO	2 liq.
A-3	10	–	–	–	–	1,200	MH	2 liq.	A-4	10	1	–	–	–	1,075	NNO	1 liq.
A-4	10	–	–	–	–	1,200	MH	2 liq.	A-1	10	1	–	–	–	1,200	QFM	2 liq.
A-5	10	–	–	–	–	1,200	MH	2 liq.	A-1	10	–	2	–	–	1,200	MH	3-liq.
A-6	10	–	–	–	–	1,200	MH	2 liq.	A-3	10	–	2	–	–	1,200	MH	3-liq.
A-1	10	–	–	–	–	1,150	MH	2 liq.	A-4	10	–	2	–	–	1,200	MH	3-liq.
A-3	10	–	–	–	–	1,150	MH	2 liq.	A-5	10	–	2	–	–	1,200	MH	3-liq.
A-5	10	–	–	–	–	1,150	MH	2 liq.	A-6	10	–	2	–	–	1,200	MH	3-liq.
A-7	10	–	–	–	–	1,150	MH	1 liq. + mt	A-1	10	–	2	–	–	1,150	MH	3-liq.
A-1	10	–	–	–	–	1,075	MH	1 liq. + mt	A-3	10	–	2	–	–	1,150	MH	3-liq.
A-3	10	–	–	–		1,075	MH	1 liq. + mt	A-5	10	–	2	–	–	1,150	MH	3-liq.
A-5	10	–	–	–	–	1,075	MH	1 liq. + mt	A-7	10	–	2	–	–	1,150	MH	2 liq. + mt
A-7	10	–	–	–	–	1,075	MH	1 liq. + mt	A-1	10	–	2	–	–	1,075	MH	1 liq. + mt + sil
A-1	10	–	–	–	–	1,200	NNO	2 liq.	A-3	10	–	2	–	–	1,075	MH	1 liq. + mt + sil
A-2	10	–	–	–	–	1,200	NNO	1 liq.	A-5	10	–	2	–	–	1,075	MH	2 liq. + mt
A-3	10	–	–	–	–	1,200	NNO	1 liq.	A-7	10	–	2	–	–	1,075	MH	2 liq. + mt
A-5	10	–	–	–	–	1,200	NNO	1 liq.	A-1	10	–	2	–	–	1,200	NNO	2 liq.
A-7	10	–	–	–	–	1,200	NNO	1 liq.	A-2	10	–	2	–	–	1,200	NNO	2 liq.
A-1	10	–	–	–	–	1,150	NNO	1 liq.	A-3	10	–	2	–	–	1,200	NNO	2 liq.
A-2	10	–	–	–	–	1,150	NNO	1 liq.	A-4	10	–	2	–	–	1,200	NNO	2 liq.
A-1	10	–	–	–	–	1,200	QFM	2 liq.	A-5	10	–	2	–	–	1,200	NNO	1 liq.
A-1	10	1	–	–	–	1,200	MH	2 liq.	A-6	10	–	2	–	–	1,200	NNO	1 liq.
A-2	10	1	–	–	–	1,200	MH	2 liq.	A-7	10	–	2	–	–	1,200	NNO	1 liq.
A-3	10	1	–	–	–	1,200	MH	2 liq.	A-1	10	–	2	–	–	1,150	NNO	2 liq.
A-4	10	1	–	–	–	1,200	MH	2 liq.	A-2	10	–	2	–	–	1,150	NNO	2 liq.
A-5	10	1	–	–	–	1,200	MH	2 liq.	A-3	10	–	2	–	–	1,150	NNO	2 liq.
A-6	10	1	–	–	–	1,200	MH	2 liq.	A-4	10	–	2	–	–	1,150	NNO	1 liq.
A-7	10	1	–	–	–	1,200	MH	1 liq.	A-1	10	–	2	–	–	1,075	NNO	2 liq.
A-1	10	1	–	–	–	1,150	MH	2 liq.	A-2	10	–	2	–	–	1,075	NNO	2 liq.
A-3	10	1	–	–	–	1,150	MH	2 liq.	A-3	10	–	2	–	–	1,075	NNO	1 liq.
A-5	10	1	–	–	–	1,150	MH	2 liq.	A-3	10	2	–	–	–	1,200	QFM	2 liq. + mt
A-7	10	1	–	–	–	1,150	MH	1 liq. + mt	A-1	10	–	–	6	–	1,200	MH	2 liq.
A-1	10	1	–	–	–	1,075	MH	2 liq. + mt	A-2	10	–	–	6	–	1,200	MH	2 liq.
A-3	10	1	–	–	–	1,075	MH	2 liq. + mt	A-3	10	–	–	6	–	1,200	MH	2 liq.
A-4	10	1	–	–	–	1,075	MH	2 liq. + mt	A-4	10	–	–	6	–	1,200	MH	2 liq.
A-7	10	1	–	–	–	1,075	MH	1 liq. + mt	A-5	10	–	–	6	–	1,200	MH	2 liq.
A-1	10	1	–	–	–	1,200	NNO	2 liq.	A-6	10	–	–	6	–	1,200	MH	1 liq.
A-2	10	1	–	–	–	1,200	NNO	2 liq.	A-1	10	–	–	6	–	1,150	MH	1 liq. + sil
A-3	10	1	–	–	–	1,200	NNO	2 liq.	A-2	10	–	–	6	–	1,150	MH	1 liq. + sil
A-4	10	1	–	–	–	1,200	NNO	2 liq.	A-3	10	–	–	6	–	1,150	MH	2 liq.
A-5	10	1	–	–	–	1,200	NNO	2 liq.	A-4	10	–	–	6	–	1,150	MH	2 liq.
A-6	10	1	–	–	–	1,200	NNO	1 liq.	A-5	10	–	–	6	–	1,150	MH	2 liq.
A-1	10	1	–	–	–	1,150	NNO	2 liq.	A-7	10	–	–	6	–	1,150	MH	1 liq. + mt
A-2	10	1	–	–	–	1,150	NNO	2 liq.	A-1	10	–	–	6	–	1,075	MH	1 liq. + sil

Table 2 continued

Base	Composition					t (°C)	Buffer	Phase assemblage	Base	Composition					t (°C)	Buffer	Phase assemblage
	Additional components (wt% base)									Additional components (wt% base)							
	H_2O	P	S	F	Cl					H_2O	P	S	F	Cl			
A-3	10	1	–	–	–	1,150	NNO	2 liq.	A-3	10	–	–	6	–	1,075	MH	2 liq. + mt
A-4	10	1	–	–	–	1,150	NNO	2 liq.	A-5	10	–	–	6	–	1,075	MH	1 liq. + mt
A-5	10	1	–	–	–	1,150	NNO	1 liq.	A-7	10	–	–	6	–	1,075	MH	1 liq. + mt
A-1	10	1	–	–	–	1,075	NNO	2 liq.	A-1	10	–	–	6	–	1,200	NNO	2 liq.
A-2	10	–	–	6	–	1,200	NNO	1 liq.	A-5	10	–	–	–	6	1,150	MH	1 liq. + mt + sil
A-3	10	–	–	6	–	1,200	NNO	1 liq.	A-6	10	–	–	–	6	1,150	MH	1 liq. + mt + sil
A-4	10	–	–	6	–	1,200	NNO	1 liq.	A-7	10	–	–	–	6	1,150	MH	1 liq. + mt + sil
A-1	10	–	–	6	–	1,150	NNO	2 liq.	An_{50}	10	–	–	–	–	1,200	NNO	2 liq.
A-2	10	–	–	6	–	1,150	NNO	1 liq.	An_{50}	10	1	–	–	–	1,200	NNO	2 liq.
A-1	10	–	–	6	–	1,200	QFM	2 liq.	An_{50}	10	–	2	–	–	1,200	NNO	2 liq.
A-1	10	–	–	–	6	1,200	MH	1 liq. + sil	An_{50}	10	–	–	6	–	1,200	NNO	2 liq.
A-2	10	–	–	–	6	1,200	MH	1 liq. + sil	A-1	–	–	–	–	–	1,200	MH	1 liq. + mt
A-3	10	–	–	–	6	1,200	MH	2 liq.	A-1	–	–	2	–	–	1,200	MH	2 liq + mt
A-4	10	–	–	–	6	1,200	MH	1 liq. + sil	A-1	–	–	–	–	6	1,200	MH	2 liq.
A-5	10	–	–	–	6	1,200	MH	1 liq. + mt + sil	A-1	–	1	–	–	–	1,200	NNO	2 liq.
A-6	10	–	–	–	6	1,200	MH	1 liq. + mt + sil	A-1	–	–	–	6	–	1,200	NNO	2 liq. + mt
A-7	10	–	–	–	6	1,200	MH	1 liq. + mt + sil	A-1	–	–	–	–	–	1,200	QFM	1 liq. + mt
A-1	10	–	–	–	6	1,150	MH	1 liq. + sil	A-1	–	1	–	–	–	1,200	QFM	2 liq.
A-2	10	–	–	–	6	1,150	MH	1 liq. + sil	A-1	–	–	–	6	–	1,200	QFM	2 liq.
A-3	10	–	–	–	6	1,150	MH	1 liq. + sil	A-1	–	–	–	–	6	1,200	QFM	2 liq. + sil

All experimental melts include a vapor phase. Data for A-2–A-6 with P, S from Lester (2002)

liq liquid, *mt* magnetite, *sil* silica minerals

$P = 200$ MPa ± 1.5

Exsolving conjugate immiscible liquids nucleate and form droplets which grow and, to varying degree, coalesce (Fig. 1a). Each liquid commonly occurs as droplets or pools distributed within a larger volume of the other liquid (Bowen 1925; Philpotts 2008). Experimental melts produced in this study in systems with H_2O alone or H_2O + P, S or F exhibit a spherical geometry similar to that observed in anhydrous melts (Fig. 1b).

All of the experimental immiscible melt phase assemblages contain a vapor phase. The presumed equilibrium vapor bubbles are generally >10 μm in diameter and are defined by menisci that appear smooth under high-power magnification. These bubbles are distinguished from quench-induced vapor exsolution textures which form as small bubbles of <1 μm or as aggregate masses of bubbles with irregular geometries.

Macroscopic-scale liquid-phase aggregation and gravitational segregation has been reported in anhydrous immiscible silicate melts (Kyser et al. 1998). In the present study, the spatial orientation of experimental capsules was recorded prior to the heating of selected charges, and the gravitational settling (density segregation) of Fe-rich immiscible liquids was evident in the run products produced in each of the H_2O-bearing experimental systems.

Addition of H_2O

H_2O-induced liquidus suppression in both natural and synthetic silicate melts is well documented (Médard and Grove 2008; Gaetani et al. 1994). In the hydrous experimental systems considered here, the H_2O-induced thermal suppression of the liquidus surfaces exposes low-temperature, compositionally extensive, two- or three-liquid miscibility gaps, some of which lie partially or entirely below the liquidus surfaces in anhydrous systems of similar compositions (Fig. 2). In the system Fe_3O_4–Fe_2O_3–$KAlSi_2O_6$–SiO_2–H_2O at fO_2 = MH, the composition range of the miscibility gap is increased relative to the range in equivalent anhydrous melts (Fig 3). The minimum temperature observed for the two-liquid field in the experimental melts with added H_2O is 1,150 °C, in anhydrous melts that are otherwise equivalent in composition, 1,375 °C (Naslund, 1983). At fO_2 = NNO, the addition of

Table 3 Electron microprobe analyses of experimental run products and major element liquid partition coefficients, $D_{Fe\text{-}liq/Si\text{-}liq}$ (wt% component in Fe-rich liquid/wt% component in silicate-rich liquid)

Starting composition	t (°C)	fO_2 buffer	Conjugate liquid	n	SiO_2	FeO	Al_2O_3	K_2O	P	S	F	Cl	Total
System: SiO_2–FeO–Al_2O_3–K_2O ± H_2O													
A-1 + H_2O	1,200	MH	Fe-liq.	5	36.54	55.98	2.91	1.18	–	–	–	–	96.64
			SD		0.21	0.35	0.32	0.10	–	–	–	–	0.32
			Sil-liq.	4	71.19	16.00	5.62	4.67	–	–	–	–	97.49
			SD		0.51	3.50	0.52	0.25	–	–	–	–	0.39
			$D_{Fe\text{-}liq/Si\text{-}liq}$		0.51	3.50	0.52	0.25	–	–	–	–	
A-3 + H_2O	1,200	MH	Fe-liq.	3	38.01	55.20	3.41	1.49	–	–	–	–	98.15
			SD		0.32	0.01	0.03	0.05	–	–	–	–	0.31
			Sil-liq.	5	76.81	9.83	6.17	5.40	–	–	–	–	98.22
			SD		0.68	0.29	0.25	0.25	–	–	–	–	0.43
			$D_{Fe\text{-}liq/Si\text{-}liq}$		0.49	5.62	0.55	0.28	–	–	–	–	
A-4 + H_2O	1,200	MH	Fe-liq.	5	45.91	44.79	4.25	2.77	–	–	–	–	97.80
			SD		0.19	0.42	0.10	0.00	–	–	–	–	0.44
			Sil-liq.	5	65.40	20.79	6.21	5.53	–	–	–	–	97.94
			SD		0.33	0.26	0.04	0.08	–	–	–	–	0.55
			$D_{Fe\text{-}liq/Si\text{-}liq}$		0.70	2.15	0.68	0.50	–	–	–	–	
A-5 + H_2O	1,200	MH	Fe-liq.	4	36.75	55.14	3.51	1.97	–	–	–	–	97.39
			SD		0.46	0.58	0.03	0.23	–	–	–	–	0.25
			Sil-liq.	5	61.70	21.27	8.06	6.81	–	–	–	–	97.89
			SD		1.22	1.40	0.17	0.22	–	–	–	–	0.14
			$D_{Fe\text{-}liq/Si\text{-}liq}$		0.60	2.59	0.44	0.29	–	–	–	–	
A-6 + H_2O	1,200	MH	Fe-liq.	3	39.31	53.51	1.87	0.99	–	–	–	–	96.48
			SD		0.59	1.36	0.20	0.24	–	–	–	–	0.50
			Sil-liq.	4	74.34	14.93	3.95	3.16	–	–	–	–	96.51
			SD		0.74	0.28	0.04	0.98	–	–	–	–	0.64
			$D_{Fe\text{-}liq/Si\text{-}liq}$		0.53	3.58	0.47	0.31	–	–	–	–	
A-1 + H_2O	1,150	MH	Fe-liq.	3	43.11	49.09	2.46	1.79	–	–	–	–	96.48
			SD		1.17	1.69	0.12	0.09	–	–	–	–	0.50
			Sil-liq.	4	76.82	8.01	5.96	5.68	–	–	–	–	96.51
			SD		1.01	1.04	0.32	0.41	–	–	–	–	0.64
			$D_{Fe\text{-}liq/Si\text{-}liq}$		0.56	6.13	0.41	0.31	–	–	–	–	
A-5 + H_2O	1,150	MH	Fe-liq.	2	51.72	34.47	6.25	4.35	–	–	–	–	96.80
			SD		1.36	1.20	0.19	0.45	–	–	–	–	0.86
			Sil-liq.	5	69.16	13.57	8.33	6.81	–	–	–	–	97.87
			SD		0.53	0.22	0.09	0.80	–	–	–	–	0.49
			$D^{Fe\text{-}liq/Si\text{-}liq}$		0.75	2.54	0.75	0.64	–	–	–	–	
A-1	1,200	MH	Fe-liq.	1	35.41	58.30	2.27	1.01	–	–	–	–	97.00
			SD						–	–	–	–	
			Sil-liq.	3	72.43	23.22	3.17	1.92	–	–	–	–	100.75
			SD		1.49	2.05	0.09	0.04	–	–	–	–	0.52
			$D_{Fe\text{-}liq/Si\text{-}liq}$		0.49	2.51	0.72	0.53	–	–	–	–	
A-1 + H_2O	1,200	NNO	Fe-liq.	5	40.1	55.7	1.91	0.76	–	–	–	–	98.52
			SD		0.83	1.17	0.18	0.14	–	–	–	–	0.53
			Sil-liq.	5	79.42	11.59	2.71	2.03	–	–	–	–	95.75
			SD		0.43	0.12	0.05	0.12	–	–	–	–	0.43
			$D_{Fe\text{-}liq/Si\text{-}liq}$		0.51	4.8	0.71	0.38	–	–	–	–	
System: SiO_2–FeO–Al_2O_3–K_2O–P ± H_2O													
A-1 + H_2O + P	1,200	MH	Fe-liq.	5	29.63	67.95	1.35	0.68	5.75	–	–	–	92.97

Table 3 continued

Starting composition	t (°C)	fO_2 buffer	Conjugate liquid	n	SiO_2	FeO	Al_2O_3	K_2O	P	S	F	Cl	Total
			SD		0.10	2.09	0.07	0.04	0.12	–	–	–	0.07
			Sil-liq.	5	75.41	7.12	2.55	2.18	0.47	–	–	–	95.40
			SD		1.53	0.10	0.02	0.44	0.10	–	–	–	0.64
			$D_{Fe\text{-}liq/Si\text{-}liq}$		0.39	9.55	0.53	0.31	12.12	–	–	–	
A-3 + H_2O + P	1,200	M-H	Fe-liq.	2	33.11	57.34	2.20	1.18	4.47	–	–	–	98.29
			SD		0.46	1.07	1.51	0.10	0.05	–	–	–	0.17
			Sil-liq.	3	80.62	2.55	3.89	2.22	0.26	–	–	–	99.54
			SD		1.58	0.27	0.91	0.78	0.08	–	–	–	0.94
			$D_{Fe\text{-}liq/Si\text{-}liq}$		0.37	22.49	0.57	0.53	17.08	–	–	–	
A-6 + H_2O + P	1,200	MH	Fe-liq.	5	20.43	59.46	2.28	0.68	2.56	–	–	–	97.80
			SD		0.15	0.49	0.04	0.05	2.09	–	–	–	0.71
			Sil-liq.	5	82.94	10.37	6.94	5.68	0.62	–	–	–	98.88
			SD		0.37	1.01	0.29	0.72	0.03	–	–	–	0.43
			$D_{Fe\text{-}liq/Si\text{-}liq}$		0.25	5.73	0.33	0.12	4.12	–	–	–	
A-2 + H_2O + P	1,150	MH	Fe-liq.	5	29.96	58.68	2.43	0.50	6.17	–	–	–	97.73
			SD		0.25	0.55	0.14	0.05	0.17	–	–	–	0.17
			Sil-liq.	5	80.46	5.99	7.15	5.00	0.53	–	–	–	99.13
			SD		1.74	0.11	0.64	1.00	0.09	–	–	–	1.00
			$D_{Fe\text{-}liq/Si\text{-}liq}$		0.37	9.79	0.34	0.10	11.68	–	–	–	
A-5 + P + H_2O	1,150	MH	Fe-liq.	3	36.85	49.47	2.79	2.20	7.18	–	–	–	98.49
			SD		2.84	3.01	0.49	0.52	0.53	–	–	–	0.50
			Sil-liq.	3	76.23	6.64	7.88	7.07	0.43	–	–	–	98.25
			SD		0.84	0.71	0.44	1.15	0.04	–	–	–	0.58
			$D_{Fe\text{-}liq/Si\text{-}liq}$		0.48	7.45	0.35	0.31	16.69	–	–	–	
A-1 + H_2O + P	1,200	MH	Fe-liq.	4	32.78	59.61	1.49	0.35	3.97	–	–	–	98.20
			SD		1.55	2.39	0.37	0.08	0.37	–	–	–	0.84
			Sil-liq.	4	83.94	8.19	2.95	2.47	0.29	–	–	–	97.70
			SD		0.86	0.61	0.14	0.63	0.21	–	–	–	1.01
			$D_{Fe\text{-}liq/Si\text{-}liq}$		0.39	7.28	0.50	0.14	13.7	–	–	–	
A-1 + H_2O + P	1,200	QFM	Fe-liq.	3	33.00	59.00	1.44	0.95	3.89	–	–	–	98.29
			SD		0.57	0.93	0.17	0.15	0.14	–	–	–	0.25
			Sil-liq.	5	77.54	11.32	4.40	4.49	0.31	–	–	–	98.06
			SD		0.41	0.61	0.17	0.45	0.05	–	–	–	0.86
A-1 + P	1,200	QFM	Fe-liq.	4	31.62	60.52	1.32	0.70	4.27	–	–	–	98.43
			SD		0.40	0.76	0.10	0.04	0.09	–	–	–	0.79
			Sil-liq.	5	77.41	11.26	4.84	4.71	0.33	–	–	–	98.55
			SD		2.16	1.25	0.48	0.86	0.02	–	–	–	0.47
			$D_{Fe\text{-}liq/Si\text{-}liq}$		0.41	5.38	0.27	0.15	12.90	–	–	–	
A-1 + H_2O + P	1,200	NNO	Fe-liq.	4	35	56.9	1.9	0.44	4.91	–	–	–	99.05
			SD		1.09	0.42	0.08	0.1	2	–	–	–	0.76
			Sil-liq.	5	76.17	12.48	2.41	1.58	0.54	–	–	–	93.17
			SD		0.45	0.34	0.04	0.05	0.08	–	–	–	0.39
			$D_{Fe\text{-}liq/Si\text{-}liq}$		0.46	4.56	0.79	0.28	8.96	–	–	–	
A-2 + H_2O + P	1,200	NNO	Fe-liq.	5	30.9	58.9	3.27	0.26	5.71	–	–	–	99.03
			SD		0.36	0.46	0.07	0.04	0.36	–	–	–	0.24
			Sil-liq.	5	76.80	9.81	6.62	4.90	0.34	–	–	–	98.46
			SD		0.64	0.42	0.14	0.07	0.05	–	–	–	1.16
			$D_{Fe\text{-}liq/Si\text{-}liq}$		0.4	6.01	0.49	0.05	6.9	–	–	–	

Table 3 continued

Starting composition	t (°C)	fO_2 buffer	Conjugate liquid	n	SiO_2	FeO	Al_2O_3	K_2O	P	S	F	Cl	Total
A-3 + H_2O + P	1,200	NNO	Fe-liq.	4	26.5	60.9	1.57	0.54	7.97	–	–	–	97.51
			SD		0.69	0.67	0.13	0.13	0.48	–	–	–	0.96
			Sil-liq.	4	74.94	11.49	4.26	3.44	0.51	–	–	–	94.64
			SD		0.27	0.18	0.12	0.05	0.03	–	–	–	0.32
			$D_{Fe\text{-}liq/Si\text{-}liq}$		0.35	5.3	0.37	0.16	15.6	–	–	–	
A-4 + H_2O + P	1,200	NNO	Fe-liq.	5	28.2	59.5	2.72	1.35	7.47	–	–	–	99.21
			SD		0.59	1.09	0.21	0.29	1.3	–	–	–	0.42
			Sil-liq.	5	74.79	9.95	6.34	5.37	0.62	–	–	–	97.08
			SD		1.36	0.95	0.58	0.23	0.15	–	–	–	0.37
			$D_{Fe\text{-}liq/Si\text{-}liq}$		0.38	5.98	0.43	0.25	12.1	–	–	–	
A-5 + H_2O + P	1,200	NNO	Fe-liq.	3	32.86	55.52	4.03	2.71	1	–	–	–	96.13
			SD		1.97	2	0.25	0.21	0.38	–	–	–	0.09
			Sil-liq.	3	65.02	18.78	7.61	5.42	2.17	–	–	–	98.99
			SD		0.55	0.53	0.06	0.07	0.06	–	–	–	0.04
			$D_{Fe\text{-}liq/Si\text{-}liq}$		0.51	2.96	0.53	0.5	0.46	–	–	–	
A-1 + H_2O + P	1,150	NNO	Fe-liq.	2	29.8	54.3	3.66	2.04	11.8	–	–	–	101.6
			SD		1.54	3.91	0.29	0.23	4.96	–	–	–	2.07
			Sil-liq.	5	66.05	17.86	7.61	5.57	2.04	–	–	–	99.12
			SD		0.58	0.27	0.07	0.05	0.08	–	–	–	0.78
			$D_{Fe\text{-}liq/Si\text{-}liq}$		0.45	3.04	0.48	0.37	5.79	–	–	–	
A-2 + H_2O + P	1,150	NNO	Fe-liq.	3	31.48	58.9	4.48	0.19	5.94	–	–	–	97.31
			SD		0.75	0.28	0.05	0.05	0.36	–	–	–	0.47
			Sil-liq.	3	79.40	10.16	6.16	3.89	0.4	–	–	–	100
			SD		0.34	0.39	0.03	0.80	0.02	–	–	–	0.37
			$D_{Fe\text{-}liq/Si\text{-}liq}$		0.40	5.44	0.73	0.05	14.8	–	–	–	
A-3 + H_2O + P	1,150	NNO	Fe-liq.	2	44.4	40.8	2.78	1.83	7.73	–	–	–	97.45
			SD		1.37	0.91	0.07	0.08	2.67	–	–	–	2.06
			Sil-liq.	2	66.47	20.15	4.21	2.72	2.06	–	–	–	95.61
			SD		0.75	1.15	0.01	0.11	0.03	–	–	–	0.32
			$D_{Fe\text{-}liq/Si\text{-}liq}$		0.67	2.02	0.66	0.67	3.76	–	–	–	
A-4 + H_2O + P	1,150	NNO	Fe-liq.	2	11.7	66.2	2.19	1	0.19	–	–	–	81.29
			SD		2.01	6.67	0	0.15	0.06	–	–	–	8.46
			Sil-liq.	3	63.07	19.75	5.46	3.05	2.41	–	–	–	93.74
			SD		0.02	0.18	0.01	0.03	0.10	–	–	–	0.08
			$D_{Fe\text{-}liq/Si\text{-}liq}$		0.19	3.35	0.4	0.33	0.08	–	–	–	
A-1 + H_2O + P	1,075	NNO	Fe-liq.	2	32	56.1	5.13	0.43	5.3	–	–	–	98.92
			SD		0.32	0.64	0.08	0.1	0.05	–	–	–	0.25
			Sil-liq.	5	73.60	9.73	8.02	5.29	0.33	–	–	–	96.97
			SD		0.63	0.61	0.10	0.08	0.11	–	–	–	0.94
			$D_{Fe\text{-}liq/Si\text{-}liq}$		0.43	5.76	0.64	0.08	15.8	–	–	–	
A-2 + H_2O + P	1,075	NNO	Fe-liq.	4	31.7	58.4	2.23	0.97	5.47	–	–	–	98.72
			SD		0.86	2.05	0.38	0.18	0.44	–	–	–	1.1
			Sil-liq.	5	76.17	8.31	5.67	4.21	0.17	–	–	–	94.53
			SD		0.87	0.11	0.07	0.09	0.03	–	–	–	0.80
			$D_{Fe\text{-}liq/Si\text{-}liq}$		0.42	7.02	0.39	0.23	33.1	–	–	–	
A-3 + H_2O + P	1,075	NNO	Fe-liq.	4	26.4	60.2	1.48	0.72	10.8	–	–	–	99.56
			SD		2.01	1.39	0.21	0.22	2.74	–	–	–	0.96
			Sil-liq.	5	77.91	9.35	6.40	5.56	0.30	–	–	–	99.52

Table 3 continued

Starting composition	t (°C)	fO_2 buffer	Conjugate liquid	n	SiO_2	FeO	Al_2O_3	K_2O	P	S	F	Cl	Total
			SD		0.62	0.62	0.07	0.06	0.09	–	–	–	0.35
			$D_{Fe\text{-}liq/Si\text{-}liq}$		0.34	6.44	0.23	0.13	35.9	–	–	–	
A-1 + P	1,200	NNO	Fe-liq.		30.6	57.9	3.01	1.04	6.25	–	–	–	98.85
			SD		1.08	3.7	1.29	0.28	1.04	–	–	–	1.44
			Sil-liq.		77.77	9.62	5.86	5.23	0.26	–	–	–	98.74
			SD		0.39	6.02	0.51	0.20	23.85	–	–	–	1.00
			$D_{Fe\text{-}liq/Si\text{-}liq}$		0.39	6.02	0.51	0.2	23.85	–	–	–	
System: SiO_2–FeO–Al_2O_3–K_2O–S ± H_2O													
A-1 + H_2O + S	1,200	MH	Fe-liq.	5	35.98	58.07	2.61	0.57	–	1.96	–	–	99.20
			SD		1.58	1.21	1.22	0.05	–	1.28	–	–	0.55
			Sil-liq.	5	86.69	7.14	2.71	2.04	–	0.06	–	–	98.64
			SD		5.75	2.56	1.57	0.95	–	0.05	–	–	1.27
			$D_{Fe\text{-}liq/Si\text{-}liq}$		0.42	8.14	0.96	0.28	–	33.09	–	–	1.01
			Sulfide	3	0.62	61.49	0.04	0.01	–	25.89	–	–	88.05
			SD		0.03	0.50	0.02	0.01	–	0.50	–	–	0.93
A-3 + H_2O + S	1,200	MH	Fe-liq.	5	30.66	62.74	2.34	0.12	–	6.29	–	–	102.16
			SD		1.02	0.42	0.29	0.01	–	0.81	–	–	0.42
			Sil-liq.	2	87.92	3.45	4.19	3.40	–	0.05	–	–	99.00
			SD		3.86	1.65	1.55	1.14	–	0.03	–	–	0.50
			$D_{Fe\text{-}liq/Si\text{-}liq}$		0.35	18.20	0.56	0.04	–	135.8	–	–	1.03
A-5 + H_2O + S	1,200	MH	Fe-liq.	5	24.24	66.73	2.05	0.16	–	10.29	–	–	103.47
			SD		0.41	0.99	0.04	0.02	–	0.10	–	–	1.41
			Sil-liq.	5	75.18	8.23	8.89	6.28	–	0.11	–	–	98.69
			SD		0.20	0.22	0.04	0.35	–	0.01	–	–	0.24
			$D_{Fe\text{-}liq/Si\text{-}liq}$		0.32	8.10	0.23	0.02	–	94.72	–	–	1.05
			Sulfide	4	1.77	60.76	0.06	0.07	–	22.68	–	–	85.34
			SD		0.10	0.15	0.01	0.01	–	1.00	–	–	0.85
A-6 + H_2O + S	1,200	MH	Fe-liq.	5	24.45	66.97	1.59	0.12	–	10.75	–	–	103.88
			SD		0.30	0.58	0.05	0.02	–	0.13	–	–	0.60
			Sil-liq.	4	73.16	8.22	9.73	7.32	–	0.35	–	–	98.79
			SD		1.07	0.81	0.20	0.15	–	0.35	–	–	0.42
			$D_{Fe\text{-}liq/Si\text{-}liq}$		0.33	8.14	0.16	0.02	–	30.95	–	–	1.05
			Sulfide	5	1.59	62.68	0.23	0.03	–	19.60	–	–	84.13
			SD		0.03	1.51	0.37	0.01	–	0.67	–	–	1.79
A-1 + H_2O + S	1,150	MH	Fe-liq.	5	40.78	51.63	3.84	1.30	–	1.69	–	–	99.24
			SD		0.89	2.87	0.05	0.09	–	0.13	–	–	1.80
			Sil-liq.	2	79.75	3.69	6.90	5.75	–	0.04	–	–	94.87
			SD		1.97	0.40	1.13	0.46	–	0.03	–	–	1.92
			$D_{Fe\text{-}liq/Si\text{-}liq}$		0.51	14.00	0.56	0.23	–	45.31	–	–	
A-3 + H_2O + S	1,150	MH	Fe-liq.	3	28.76	63.37	3.09	0.19	–	8.33	–	–	103.74
			SD		0.47	0.43	0.10	0.02	–	0.28	–	–	0.28
			Sil-liq.	5	73.77	9.04	8.98	6.84	–	0.13	–	–	98.76
			SD		0.42	0.24	0.11	0.11	–	0.01	–	–	0.27
			$D_{Fe\text{-}liq/Si\text{-}liq}$		0.39	7.01	0.34	0.03	–	65.57	–	–	1.05
A-5 + H_2O + S	1,150	MH	Fe-liq.	5	32.77	60.33	2.76	1.57	–	2.46	–	–	99.89
			SD		1.08	0.65	0.43	0.18	–	0.99	–	–	0.85
			Sil-liq.	4	67.56	12.12	10.67	8.88	–	0.12	–	–	99.35
			SD		1.61	1.34	0.25	0.52	–	0.01	–	–	0.72

Table 3 continued

Starting composition	t (°C)	fO_2 buffer	Conjugate liquid	n	SiO_2	FeO	Al_2O_3	K_2O	P	S	F	Cl	Total
			$D_{Fe\text{-}liq/Si\text{-}liq}$		0.49	4.98	0.26	0.18	–	20.82	–	–	1.01
A-1 + H_2O + S	1,200	NNO	Fe-liq.	5	43.99	44	2.19	1	–	1.16	–	–	92.69
			SD		1.21	3.34	0.17	0.09	–	0.29	–	–	3.09
			Sil-liq.	5	77.3	15.4	2.41	1.52	–	0.21	–	–	96.84
			SD		0.63	0.56	0.03	0.07	–	0.05	–	–	0.30
			$D_{Fe\text{-}liq/Si\text{-}liq}$		0.57	2.85	0.91	0.66	–	5.64	–	–	
A-2 + H_2O + S	1,200	NNO	Fe-liq.	3	26.5	61.7	1.31	0.8	–	8.77	–	–	99.11
			SD		0.29	0.52	0.12	0.01	–	0.17	–	–	0.46
			Sil-liq.	5	73.42	13.09	5.68	5.49	–	0.68	–	–	98.37
			SD		1.54	1.07	0.17	0.17	–	0.11	–	–	0.20
			$D_{Fe\text{-}liq/Si\text{-}liq}$		0.36	4.71	0.15	0.15	–	13	–	–	
A-3 + H_2O + S	1,200	NNO	Fe-liq.	4	23.7	69.3	1.52	0.59	–	8.16	–	–	103.2
			SD		1.1	1.86	0.11	0.2	–	1.32	–	–	1.65
			Sil-liq.	4	68.76	18.46	6.21	3.52	–	0.62	–	–	97.58
			SD		2.00	2.63	0.17	0.17	–	0.07	–	–	0.99
			$D_{Fe\text{-}liq/Si\text{-}liq}$		0.34	3.75	0.24	0.17	–	13.1	–	–	
A-4 + H_2O + S	1,200	NNO	Fe-liq.	5	22.9	69	0.8	0.5	–	6.98	–	–	100.14
			SD		1.09	2.1	0.03	0.11	–	1.43	–	–	1.14
			Sil-liq.	5	69.44	18.40	4.32	3.12	–	0.56	–	–	95.85
			SD		1.26	2.25	0.08	0.17	–	0.06	–	–	1.55
			$D_{Fe\text{-}liq/Si\text{-}liq}$		0.33	3.75	0.18	0.16	–	12.4	–	–	
A-1 + H_2O + S	1,150	NNO	Fe-liq.	3	25.6	68.3	1.06	0.21	–	8.29	–	–	103.43
			SD		1.2	2.43	0.12	0.09	–	1.25	–	–	0.44
			Sil-liq.	4	83.38	7.94	2.43	1.72	–	0.15	–	–	95.61
			SD		0.36	0.20	0.08	0.02	–	0.01	–	–	0.19
			$D_{Fe\text{-}liq/Si\text{-}liq}$		0.31	8.6	0.44	0.12	–	56.6	–	–	
A-2 + H_2O + S	1,150	NNO	Fe-liq.	3	35.9	57.7	2.41	0.95	–	2.57	–	–	99.54
			SD		1.17	1.41	0.2	0.12	–	0.33	–	–	1.1
			Sil-liq.	5	73.34	16.94	3.83	2.01	–	0.32	–	–	96.44
			SD		0.80	1.37	0.07	0.05	–	0.07	–	–	0.78
			$D_{Fe\text{-}liq/Si\text{-}liq}$		0.49	3.41	0.63	0.47	–	8.13	–	–	
A-3 + H_2O + S	1,150	NNO	Fe-liq.	3	25.8	69.2	1.26	0.25	–	6.95	–	–	103.45
			SD		0.93	0.16	0.09	0.08	–	0.63	–	–	1.13
			Sil-liq.	5	76.05	11.73	4.67	3.55	–	11.73	–	–	96.37
			SD		0.80	0.95	0.04	0.10	–	0.95	–	–	0.44
			$D_{Fe\text{-}liq/Si\text{-}liq}$		0.34	5.9	0.27	0.07	–	5.9	–	–	
A-4 + H_2O + S	1,150	NNO	Fe-liq.		29.4	64.5	1.81	0.73	–	4.87	–	–	101.23
			SD		0.28	0.35	0.03	0.05	–	0.3	–	–	0.25
			Sil-liq.		70.19	15.48	6.39	4.60	–	0.29	–	–	96.69
			SD		0.44	0.71	0.07	0.11	–	0.01	–	–	0.18
			$D_{Fe\text{-}liq/Si\text{-}liq}$		0.42	4.16	0.28	0.16	–	16.7	–	–	
A-1 + H_2O + S	1,075	NNO	Fe-liq.	5	7.14	72.8	0.7	0.12	–	16.6	–	–	97.3
			SD		3.32	2.85	0.59	0.08	–	16.31	–	–	9.48
			Sil-liq.	3	82.17	7.24	3.05	1.66	–	0.28	–	–	94.40
			SD		0.14	0.60	0.04	0.06	–	0.13	–	–	0.70
			$D_{Fe\text{-}liq/Si\text{-}liq}$		0.09	10.1	0.23	0.07	–	59.2	–	–	
A-2 + H_2O + S	1,075	NNO	Fe-liq.		34	59.6	1.97	0.57	–	6.68	–	–	102.75
			SD		2.12	2.63	0.15	0.02	–	0.91	–	–	0.92

Table 3 continued

Starting composition	t (°C)	fO_2 buffer	Conjugate liquid	n	SiO_2	FeO	Al_2O_3	K_2O	P	S	F	Cl	Total
			Sil-liq.		79.71	9.29	4.00	1.86	–	0.27	–	–	95.14
			SD		0.51	1.18	0.11	0.06	–	0.21	–	–	1.36
			$D_{Fe\text{-}liq/Si\text{-}liq}$		0.43	6.41	0.49	0.31	–	24.62	–	–	
System: SiO_2–FeO–Al_2O_3–K_2O–F ± H_2O													
A-1 + H_2O + F	1,200	MH	Fe-liq.	3	34.73	60.91	2.09	0.31	–	–	5.15	–	99.70
			SD		1.44	0.21	0.25	0.04	–	–	0.26	–	1.50
			Sil-liq.	5	62.22	12.33	5.67	4.36	–	–	4.99	–	88.95
			SD		0.69	0.87	0.24	0.52	–	–	0.31	–	0.42
			$D_{Fe\text{-}liq/Si\text{-}liq}$		0.56	4.94	0.37	0.07	–	–	1.03	–	
A-2 + H_2O + F	1,200	MH	Fe-liq.	4	34.10	60.83	2.19	0.32	–	–	1.61	–	99.04
			SD		0.35	0.10	0.13	0.03	–	–	0.22	–	0.26
			Sil-liq.	5	73.98	13.16	5.37	5.29	–	–	1.27	–	99.06
			SD		0.76	0.52	0.04	0.21	–	–	0.08	–	0.44
			$D_{Fe\text{-}liq/Si\text{-}liq}$		0.46	4.62	0.41	0.06	–	–	1.27	–	
A-3 + H_2O + F	1,200	MH	Fe-liq.	3	44.63	48.47	3.49	1.74	–	–	0.13	–	98.47
			SD		0.36	0.60	0.02	0.05	–	–	0.05	–	0.30
			Sil-liq.	3	74.41	8.48	6.53	*	–	–	0.16	–	89.59
			SD		0.22	0.34	0.02	*	–	–	0.07	–	0.43
			$D_{Fe\text{-}liq/Si\text{-}liq}$		0.60	5.72	0.53	*	–	–	0.82	–	
A-4 + H_2O + F	1,200	MH	Fe-liq.	5	34.86	60.18	1.61	0.83	–	–	1.50	–	98.97
			SD		0.08	0.40	0.13	0.09	–	–	0.11	–	0.18
			Sil-liq.	5	77.19	7.67	6.24	6.11	–	–	2.98	–	100.20
			SD		0.49	0.34	0.04	0.03	–	–	0.07	–	0.41
			$D_{Fe\text{-}liq/Si\text{-}liq}$		0.45	7.84	0.26	0.14	–	–	0.50	–	
A-5 + H_2O + F	1,200	MH	Fe-liq.	5	61.47	20.00	7.38	5.71	–	–	1.66	–	99.71
			SD		1.08	1.67	0.15	0.22	–	–	0.22	–	0.44
			Sil-liq.	5	77.66	0.44	9.69	6.77	–	–	4.37	–	99.55
			SD		0.31	0.03	0.06	0.24	–	–	0.91	–	0.32
			$D_{Fe\text{-}liq/Si\text{-}liq}$		0.79	45.72	0.76	0.84	–	–	0.38	–	
A-3 + H_2O + F	1,150	MH	Fe-liq.	5	32.63	59.29	2.12	0.93	–	–	5.61	–	100.59
			SD		1.25	0.80	0.17	0.13	–	–	1.24	–	0.66
			Sil-liq.	3	78.34	6.28	5.92	4.50	–	–	5.45	–	100.48
			SD		0.73	0.06	0.08	0.66	–	–	0.11	–	0.43
			$D_{Fe\text{-}liq/Si\text{-}liq}$		0.42	9.44	0.36	0.21	–	–	1.03	–	
A-4 + H_2O + F	1,150	MH	Fe-liq.	4	34.24	57.83	1.14	0.48	–	–	5.16	–	98.86
			SD		0.25	0.10	0.01	0.13	–	–	0.34	–	0.07
			Sil-liq.	4	82.07	6.98	3.56	1.89	–	–	4.58	–	94.55
			SD		0.57	0.13	0.58	0.50	–	–	0.07	–	1.27
			$D_{Fe\text{-}liq/Si\text{-}liq}$		0.42	8.28	0.32	0.25	–	–	1.13	–	
A-5 + H_2O + F	1,150	MH	Fe-liq.	4	40.21	50.76	3.64	2.22	–	–	3.05	–	99.89
			SD		0.40	1.73	0.36	0.34	–	–	0.24	–	0.96
			Sil-liq.	5	66.22	13.51	8.39	7.36	–	–	4.83	–	100.32
			SD		0.30	0.19	0.09	0.04	–	–	0.09	–	0.44
			$D_{Fe\text{-}liq/Si\text{-}liq}$		0.61	3.76	0.43	0.30	–	–	0.63	–	
A-1 + H_2O + F	1,200	QFM	Fe-liq.	2	37.68	46.47	1.08	0.84	–	–	1.70	–	87.78
			SD		4.14	12.38	0.12	0.04	–	–	0.11	–	7.97
			Sil-liq.	2	84.21	10.73	2.63	1.63	–	–	5.60	–	96.40
			SD		0.94	0.04	0.02	0.57	–	–	0.04	–	0.39

Table 3 continued

Starting composition	t (°C)	fO_2 buffer	Conjugate liquid	n	SiO_2	FeO	Al_2O_3	K_2O	P	S	F	Cl	Total
			$D_{Fe\text{-}liq/Si\text{-}liq}$		0.45	4.33	0.41	0.52	–	–	0.30	–	
A-1 + F	1,200	QFM	Fe-liq.	2	41.02	49.57	1.44	0.86	–	–	1.72	–	94.60
			SD		4.66	1.34	0.09	0.00	–	–	0.05	–	3.45
			Sil-liq.	3	72.32	15.24	2.56	1.39	–	–	5.12	–	96.63
			SD		0.63	1.03	0.23	0.47	–	–	0.04	–	0.51
			$D_{Fe\text{-}liq/Si\text{-}liq}$		0.57	3.25	0.56	0.61	–	–	0.34	–	
A-1 + F + H_2O	1,200	NNO	Fe-liq.	3	32.21	57.80	1.86	0.96	–	–	0.69	–	93.54
			SD		0.59	0.78	0.05	0.08	–	–	0.33	–	0.00
			Sil-liq.	5	83.18	7.62	2.65	2.77	–	–	1.06	–	97.28
			SD		0.25	0.08	0.12	0.02	–	–	0.06	–	0.19
			$D_{Fe\text{-}liq/Si\text{-}liq}$		0.39	7.59	0.70	0.35	–	–	0.65	–	
System: SiO_2–FeO–Al_2O_3–K_2O–Cl ± H_2O													
A-1 + H_2O + Cl	1,200	NNO	Fe-liq.	5	39.15	50.11	2.83	1.00	–	–	–	0.02	93.11
			SD		0.48	1.08	0.08	0.06	–	–		0.03	0.86
			Sil-liq.	5	71.59	16.66	3.63	3.45	–	–	–	0.08	99.31
			SD		0.30	0.16	0.03	0.10	–	–		0.05	0.26
			$D_{Fe\text{-}liq/Si\text{-}liq}$		0.55	3.01	0.78	0.29	–	–		0.30	
System: SiO_2–FeO–Al_2O_3–K_2O–Na–Ca + H_2O ± (P, S, or F)													
An_{50} + H_2O	1,200	M-H	Fe-liq.	3	41.31	49.43	2.13	1.34	0.19	0.63	–	–	95.07
			SD		0.52	0.36	0.07	0.04	0.03	0.02	–	–	0.39
			Sil-liq.	5	74.55	14.02	3.94	3.89	0.41	0.20	–	–	97.03
			SD		0.62	0.49	0.14	0.19	0.04	0.01	–	–	0.74
			$D_{Fe\text{-}liq/Si\text{-}liq}$		0.55	3.53	0.54	0.35	0.45	3.15	–	–	
An_{50} + H_2O + P	1,200	MH	Fe-liq.	2	20.71	72.25	1.32	0.50	0.13	0.14	1.84	–	96.94
			SD		1.46	1.70	0.05	0.06	0.03	0.00	0.11	–	0.27
			Sil-liq.	5	85.26	6.25	2.44	2.25	0.23	0.06	0.31	–	96.83
			SD		0.16	0.07	0.04	0.08	0.04	0.01	0.02	–	0.14
			$D_{Fe\text{-}liq/Si\text{-}liq}$		0.24	11.57	0.54	0.22	0.59	2.26	5.90	–	
An_{50} + H_2O + S	1,200	MH	Fe-liq.	5	81.96	7.40	3.08	1.77	0.20	0.36	–	0.10	87.13
			SD		0.84	0.33	0.60	0.02	0.03	0.01	–	0.10	0.06
			Sil-liq.	5	35.52	44.24	2.46	0.38	0.09	1.72	–	0.27	86.52
			SD		3.12	2.63	0.53	0.06	0.03	0.13	–	0.01	0.10
			$D_{Fe\text{-}liq/Si\text{-}liq}$		0.43	5.98	0.80	0.21	0.46	4.75	–	2.72	
An_{50} + H_2O + F	1,200	MH	Fe-liq.	4	37.86	49.75	2.06	0.70	0.17	1.52	–	2.51	94.58
			SD		2.53	1.34	0.40	0.21	0.07	0.91	–	1.48	1.53

Asterisk signifies that the value is below the detaction limit of the instrument

H_2O to the system Fe_3O_4–$KAlSi_2O_6$–SiO_2 displaces the range of the miscibility gap to higher SiO_2 compositions and presumably extends the two-liquid field outside of the experimental composition range. A single experiment performed at fO_2 = QFM, with base composition A-1 + H_2O (10 wt%), P = 200 MPa and T = 1,200 °C, produced two conjugate liquids. The A-1 base mixture used in the experiment is more SiO_2-rich (~5 wt%) than the most SiO_2-rich parental melt in equivalent anhydrous melts, suggesting that the miscibility gap either expands or shifts toward more SiO_2-rich compositions in hydrous melts at fO_2 = QFM.

Addition of H_2O and phosphorus

The miscibility gap in the system Fe_3O_4–Fe_2O_3–$KAlSi_2O_6$–SiO_2–H_2O–P, fO_2 = MH (Fig. 2c), shows the same range of composition as that in the melts with H_2O alone, but the extent of the two-liquid plus magnetite field is significantly increased in the phosphorus-bearing system. In the system Fe_3O_4–$KAlSi_2O_6$–SiO_2–H_2O–P at fO_2 = NNO (Fig. 2d), the two-liquid field is shifted toward higher SiO_2 compositions but to a lesser degree than in melts with H_2O only. The temperatures of the magnetite saturation in

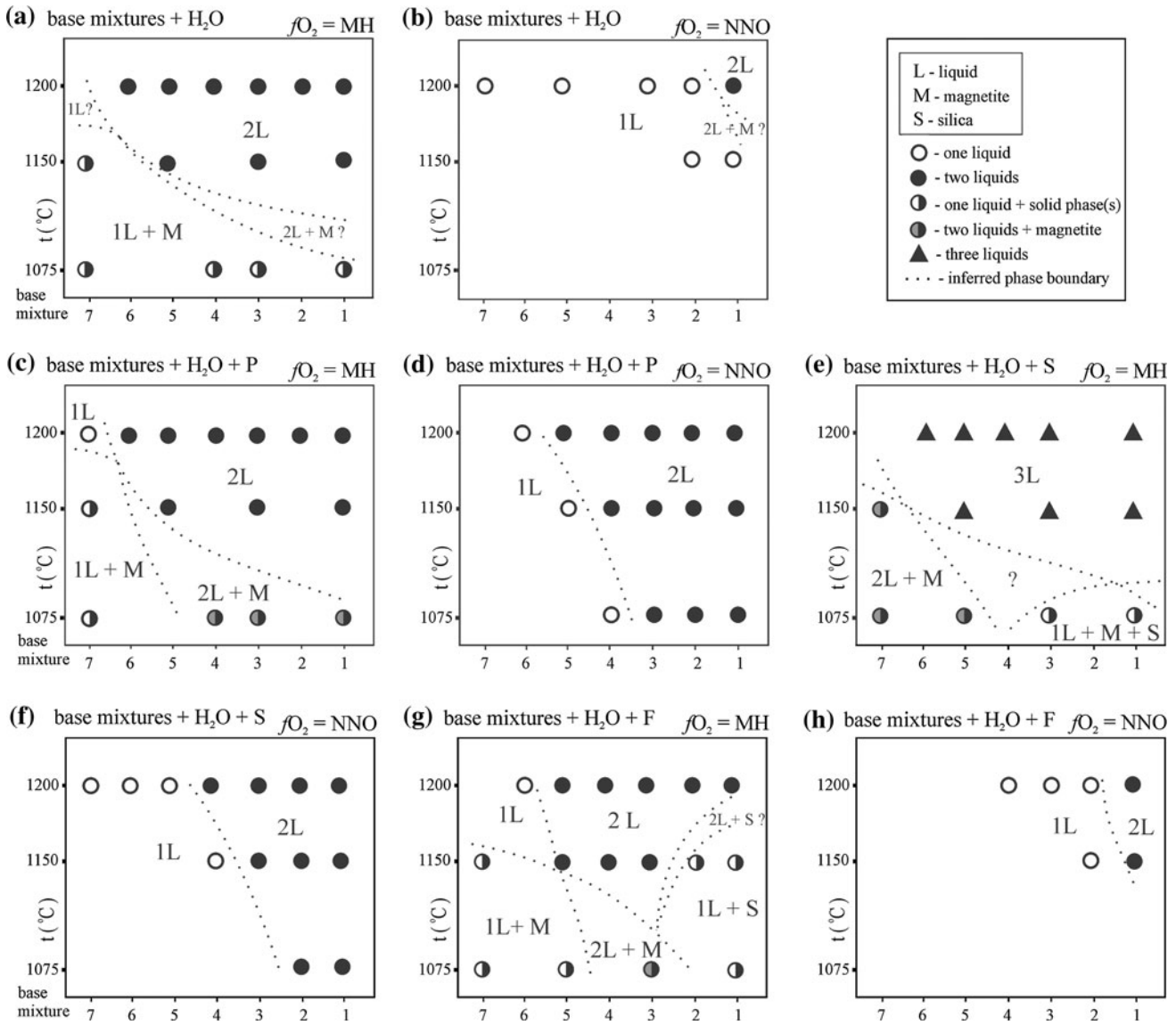

Fig. 2 Phase relations in experimental melts (**a–h**). Composition: base mixtures A-1–A-7 systems Fe_3O_4–$KAlSi_2O_6$–SiO_2 and Fe_3O_4–Fe_2O_3–$KAlSi_2O_6$–SiO_2 plus 10 wt% H_2O and either 1 wt% phosphorus, 2 wt% sulfur or 6 wt% fluorine. Conditions of experiments: T = 1,075, 1,150 or 1,200 °C, P = 200 MPa, duration—2 h, fO_2–NNO or MH buffers. *Dashed lines* represent the inferred region of phase-field boundaries

the system at fO_2 = NNO are predictably lower than at fO_2 = MH, and consequently, the two-liquid field is thus extended to lower temperatures at more reducing conditions.

Addition of H_2O and sulfur

Immiscibility between silicate and sulfide melts is well documented (e.g., Naldrett 2005), but no experimental investigations of the effect of sulfur on liquid-phase separation in silicate melts have been documented. Laroque and Stimac (2000) reported the conversion of Fe-sulfide melts to Fe-oxide melts in basaltic, intermediate and granitic systems, providing chemical and textural evidence that immiscible FeO-rich liquids are widely produced from sulfide liquids as a consequence of sulfur loss during magma devolatilization. The addition of H_2O + 2 wt% S to the system Fe_3O_4–Fe_2O_3–$KAlSi_2O_6$–SiO_2–H_2O at fO_2 = MH stabilizes a three-liquid field (Fig. 2e), a Fe-rich mafic silicate liquid, a Fe-poor felsic silicate liquid and a Fe-sulfide liquid (FeS_{63}–FeS_{74}). The three-liquid field range extends from base composition A-1 to A-6, delimited, in the low-silica portion of the experimental field, by a region in which two liquids plus magnetite are stable (Fig. 2e). The three liquids are preserved in experimental glasses as spheroidal droplets, each distributed within the other two, or as crystalline Fe-sulfide that nucleated and

grew rapidly in the sulfide liquid upon quench. The sulfide solid phase shows dendritic growth habit and is best developed on the boundary surface between magnetite crystals in some of the quenched mafic conjugate liquids (Fig. 1c).

Experiments in the system Fe_3O_4–$KAlSi_2O_6$–SiO_2–H_2O–S at fO_2 = NNO did not reach sulfide liquid saturation, but a compositionally extensive, two-liquid field stable below 1,075 °C is observed in the intermediate- to high-silica portion of the experimental composition range (Fig. 2f).

At fO_2 = NNO, the mafic liquids in the two-liquid portion of the system accommodate over 10 wt% sulfur. At fO_2 = MH, sulfur is strongly partitioned into the Fe–S–O melt, which accommodates up to 23 wt% S and 60–65 wt% FeO_{total}. The phase relations in the high-silica portion of the system Fe_3O_4–Fe_2O_3–$KAlSi_2O_6$–SiO_2–H_2O–S at fO_2 = MH, i.e., between the three-liquid field and the assemblage one liquid + magnetite + silica in temperature range of temperature range 1,075–1,150 °C, are undetermined. The exsolution of a sulfide liquid in the S-bearing melts is notable, in part, because sulfate is commonly considered the predominant sulfur specie in silicate melts under oxygen fugacity conditions above NNO, e.g., Wallace and Carmichael 1994. The assumption of equilibrium fO_2 conditions is supported by the partitioning trends of S in the two-melt fields, as well as composition data from reversal experiments. The simplest explanation for the presence of sulfide is that the speciation of sulfur is controlled by the amount of Fe^{2+} in the melts, which in turn is probably elevated because of the lack of mono- and divalent cations required to charge-balance any network-forming Fe^{3+} in the melts.

The addition of H_2O and fluorine

The addition of fluorine to the system Fe_3O_4–Fe_2O_3–$KAlSi_2O_6$–SiO_2–H_2O at fO_2 = MH increases both the composition range and the silica mineral saturation surface temperatures in the experimental regime (Fig. 2g) in agreement with the general principles of the acid–base equilibrium. A similar effect of the addition of F has been observed in the haplogranitic system, e.g., Manning (1981).

The expansion of the silica mineral stability region limits the extent of the two-liquid field and shifts the composition range of the miscibility gap to more intermediate-silica compositions. The two-liquid field in the system Fe_2O_3–$KAlSi_2O_6$–SiO_2–H_2O–F at fO_2 = NNO is limited to high-silica compositions ($\sim$66 wt% SiO_2).

The addition of H_2O and chlorine

No two-liquid field was observed in this study in the system Fe_3O_4–$KAlSi_2O_6$–SiO_2–H_2O–Cl, fO_2 = NNO. The addition of H_2O + Cl to the Fe_3O_4–Fe_2O_3–$KAlSi_2O_6$–SiO_2–H_2O fO_2 = MH system increases the temperatures of the silica mineral saturation surface to the extent that two liquids were observed only in base composition A-1 + H_2O + Cl at 1,200 °C (Table 2). Melts produced from starting mixtures of mafic to intermediate composition become significantly enriched with iron (40–64 wt% FeO_{total}) and H_2O with decreasing temperature and the progressive crystallization of silica minerals.

The addition of H_2O plus P, S, F or Cl to the system Fe_3O_4–$KAlSi_2O_6$–SiO_2–$Ca_{0.5}Na_{.5}Al_{1.5}Si_{2.5}O_8$

Experiments were performed in the system Fe_3O_4–$KAlSi_2O_6$–SiO_2–$Ca_{0.5}Na_{.5}Al_{1.5}Si_{2.5}O_8$ (An_{50}) with 10 wt% H_2O, 1 wt% P, 2 wt% S and 6 wt% F or Cl at 1,200 °C, fO_2 = NNO and P = 200 MPa. Stable two-liquid assemblages were observed in the melts with H_2O alone and with H_2O and P, S or F (Table 2). No liquid-phase separation was observed in the melts with H_2O plus Cl.

Additional experiments

Additional experiments were performed using base compositions A-1 or A-3 with or without H_2O, at 1,200 °C, P = 200 MPa and fO_2 = QFM, NNO or MH (Table 2). Two-liquid assemblages were observed in melts with compositions A-1 + H_2O (QFM), A-1 + H_2O + F (QFM), A-1 + P (QFM), A-1 + F (QFM) and A-1 + Cl (MH). Two-liquid- plus solid-phase assemblages were produced in melts A-3 + H_2O + P (QFM), A-1 + Cl (QFM), A-1 + F (NNO) and A-1 + S (MH).

Discussion

Effects of H_2O, P, S, F and Cl on the *T*–*X* range of two-liquid fields

The temperature and compositional ranges of two-liquid fields in silicate melts are dependent on the position and configuration of the miscibility gap relative to the saturation surfaces of liquidus minerals. The phase relations given in Fig. 2 reflect the combined and, in some instances, competing effects of H_2O and P, S or F on the liquidus surface configuration in each of the experimental systems. Water has the most pronounced effects on the phase relations in the experimental compositions. Thus, the addition of H_2O dramatically suppresses liquidus surface temperatures, expands the stability field of magnetite and decreases that of silica minerals, thereby increasing the *T*–*X* range of the miscibility gap (Fig. 3). In anhydrous melts in the systems Fe_2SiO_4–$KAlSi_2O_6$–SiO_2 and Fe_2SiO_4–$KAlSi_3O_8$–

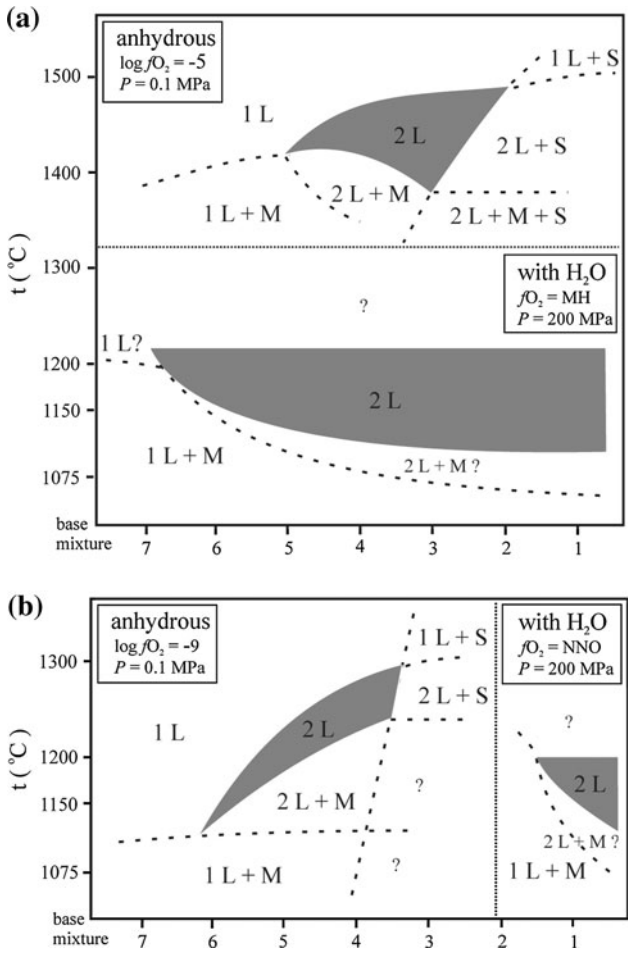

Fig. 3 Phase relations in experimental melts with 10 wt% H_2O and from equivalent anhydrous melts (Naslund 1983). **a** Phase assemblages of experimental melts with equivalent compositions run at oxygen fugacity conditions of MH buffer (this study), fixed at log $fO_2 = -5$ (Naslund). **b** Experimental melts with equivalent compositions run at oxygen fugacity conditions of NNO buffer (this study), fixed at log $fO_2 = -9$ (Naslund). *L* liquid, *M* magnetite, *S* silica mineral

SiO_2, with or without CaO, TiO_2 and MgO, the addition of phosphorus expands the two-melt field, decreasing the extent of the fayalite field and increasing that of silica minerals (Bogaerts and Schmidt 2006). It is likely that P and S (at concentrations below sulfide saturation) have a similar effect on the H_2O-rich melts in the simplified systems considered here, but H_2O-induced suppression of the silicate–mineral liquidus surface limits the stability of silica minerals to high SiO_2 compositions at low temperatures in the S-bearing melts and eliminates it altogether in the P-bearing melts. In contrast, F increases the silica mineral stability field to the extent that the two-liquid field is truncated by the silica–mineral saturation surface.

Major element partitioning and melt structure relations in volatile-rich melts

Major element partitioning trends in the volatile-rich experimental melts are similar to those reported in equivalent anhydrous melts (Watson 1976b; Naslund 1983; Bogaerts and Schmidt 2006); Fe, Ca and P preferentially partition into the mafic melt and Si, Al, K and Na into the felsic. No data have been recorded regarding the partitioning of S and F between anhydrous immiscible silicate melts, but in the H_2O-bearing melts produced in this study, S partitions strongly into the mafic melt (Fig. 4b). In contrast, F partitions nearly equally into the mafic and silicate liquids ($D_F = 1 \pm 0.6$). The absolute values of major element partition coefficients between coexisting experimental melts are generally higher than in equivalent anhydrous melts.

The relationship between major element partition ratios and melt structure in immiscible silicate melts has been used to assess the role of liquid-phase separation in the evolution of coexisting silicate magmas of differing composition. Specifically, major element mass partition ratios (D_i) plotted as a function of the melt polymerization parameter nbo/t^f (nbo number of non-bridging oxygens; t tetrahedrally coordinated network-forming cations; $f =$ the felsic member of conjugate immiscible liquids pairs) define power-law relationships that are distinct from those for coexisting melt pairs that have not undergone liquid-phase separation. Bogaerts and Schmidt (2006) demonstrated that power-law curves (for D_i as a function of nbo/t) for the elements Fe, Ti, P, Si and K for immiscible melts of basaltic composition can be applied as a means to assess rocks formed from coexisting magmas over a wide range of compositions and petrogenetic conditions.

To test whether the power-law relationships for major element partition data and nbo/t^f in anhydrous silicate melts (described above) can be applied to the assessment of melts with H_2O, P, S or F, D_i values for several of the elements are plotted as a function of the nbo/t^f values of the volatile-rich melts produced in this study (Fig. 4). For purposes of comparison, nbo/t^f values are calculated using the method of Bogaerts and Schmidt (2006), in which $t = Si + Al + P$, and all Fe is treated as a network modifier, an assumption, justified in part, because the Al/K = 1 molar ratio in the experimental melts severely limits the number of cations available to charge-balance any network-forming Fe^{3+}. Water is not included in the nbo/t^f calculation scheme because its concentration in both natural and synthetic melts is difficult to quantify and the method would be impractical if the power-law relationship between partitioning and the nbo/t^f parameter were strongly dependent upon the H_2O content of the melt.

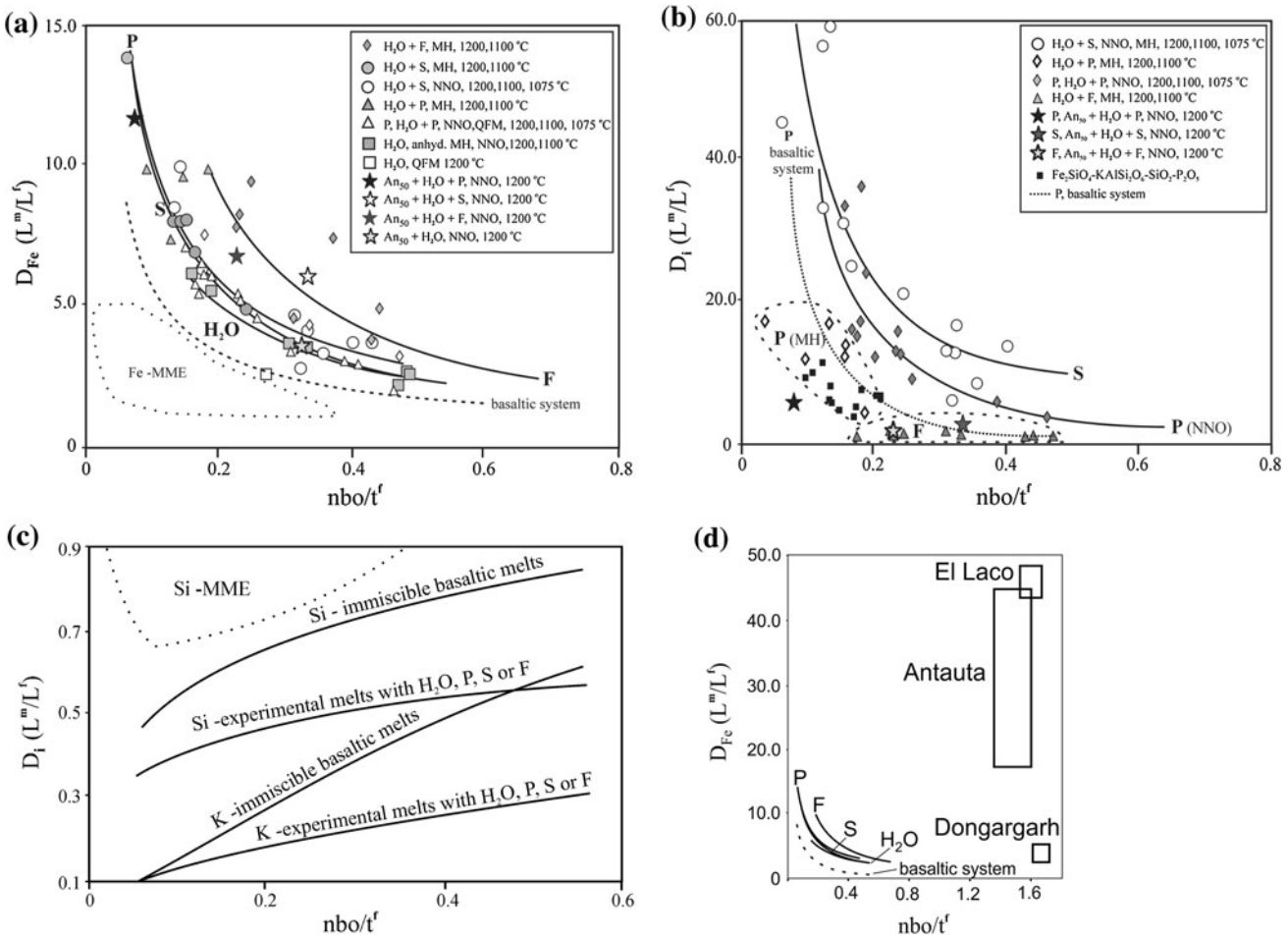

Fig. 4 Partition coefficients and nbo/t^f between conjugate experimental melts (L^m, FeO-rich melt; L^f, SiO_2-rich melt). **a** variation in the partition coefficients between melts for Fe as a function of nbo/t^f, **b** variation in the partition coefficients between melts for P, S and F as a function of nbo/t^f, literature data for P in the system Fe_2SiO_4–$KAlSi_2O_6$–SiO_2 are from Visser and Koster van Groos (1979b, c) and Freestone and Powell (1983), data for the basaltic system (tholeiitic and lunar basalts) are from Rutherford et al. (1974), Ryerson and Hess (1980), Dixon and Rutherford (1979), Ryerson and Hess (1980), Philpotts and Doyle (1983) and Longhi (1990), modified from Bogaerts and Schmidt (2006). MME partition data from non-equilibrium, coexisting microgranular enclaves in granitic melts (Bogaerts and Schmidt 2006). **c** Variation in the partition coefficients between melts for Si and K as a function of nbo/t^f in experimental melts with H_2O and H_2O plus P, S or F (this study), and in immiscible basaltic melts (Bogaerts and Schmidt 2006). **d** Fe partition coefficients between melts as a function of nbo/t^f for coexisting melt inclusions in rocks from El Laco Fe-oxide deposit, Chile; Antauta hypabyssal complex of the Picotani Group, Peru; and the Dongargarh Supergroup, India (Naslund et al. 2002; Clark and Kontak 2004; Sensarma et al. 2000)

Fe, Si and K partitioning

D_{Fe} and nbo/t data in melts with H_2O only, with P or S, overlap (Fig. 4a), yielding power-law curves which are indistinguishable from each other. Power-law equations fitting the data are as follows: for melts with H_2O only, $D_{Fe} = 1.29\ (\text{nbo}/t^f)^{-0.84}$ ($r^2 = 0.82$), for melts with H_2O + P, $D_{Fe} = 1.22\ (\text{nbo}/t^f)^{-0.95}$ ($r^2 = 0.82$) and for melts with S, $D_{Fe} = 1.62\ (\text{nbo}/t^f)^{-0.82}$ ($r^2 = 0.93$). The curve for D_{Fe} as a function of nbo/t^f in F-bearing melts differs from the curves calculated for melts with H_2O, S or P reflecting both higher D_{Fe} values and a shift in the miscibility gap toward more polymerized compositions (Fig. 5). The power-law equation fitting the data for F-bearing melts is $D_{Fe} = 1.75\ (\text{nbo}/t^f)^{-0.99}$ ($r^2 = 0.74$).

The addition of plagioclase (An_{50}) to melts with H_2O, or without H_2O plus P or F, does not induce significant changes in Fe partitioning, but D_{Fe} values in melts with plagioclase and S are greater than D_{Fe} values for the plagioclase-bearing melts with H_2O, or H_2O plus P or F. Temperature and oxygen fugacity have a minimal effect on the relationship between Fe partitioning and nbo/t in both the volatile-rich experimental melts and similar anhydrous immiscible melts (Bogaerts and Schmidt 2006).

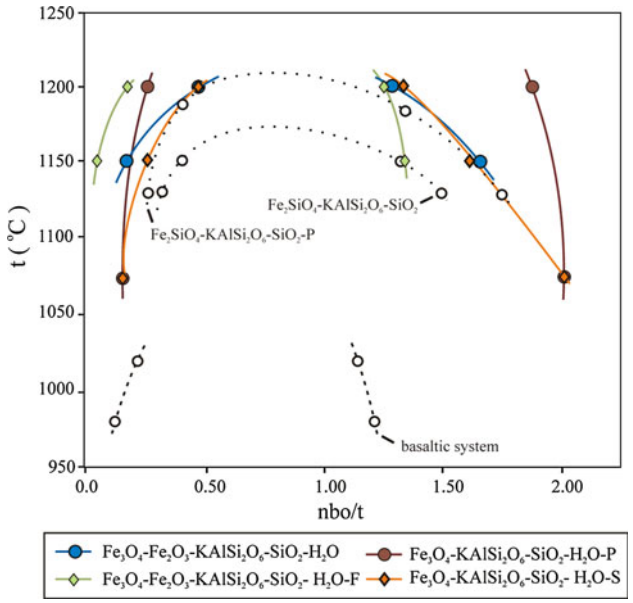

Fig. 5 Width of the miscibility gap expressed as a function of temperature plotted against nbo/*t* of conjugate liquid pairs in experimental melts with H_2O, and H_2O with P, S or F. Data for the basaltic system are from Ryerson and Hess (1980), for the systems Fe_2SiO_4–$KAlSi_2O_6$–SiO_2–P, Visser and Koster van Groos (1979b, c), modified from Bogaerts and Schmidt (2006), and for the system Fe_2SiO_4–$KAlSi_2O_6$–SiO_2, Bogaerts and Schmidt (2006)

Partitioning data for Si and K in melts with H_2O, P, S or F show significant overlap and are more dispersed than those for Fe, but data for D_{Si} as a function of nbo/t^f in the experimental melts considered in toto yield a power-law curve that is clearly distinct from that defined by Si in coexisting melts that have not undergone liquid-phase separation (Fig. 4c).

Partitioning of P, S and F

Power-law curves for D_S (fO_2 = NNO or MH) and D_P (fO_2 = NNO) in the experimental melts are similar to those for D_{Fe} and plot above the curve for D_P in immiscible basaltic liquids (Fig. 4b). Partitioning coefficient values (D_P) at fO_2 = MH are greater than D_P at fO_2 = NNO, but increased polymerization of the felsic melt shifts the D_P–nbo/t^f field toward more polymerized compositions that plot closer to the power-law curve for P in immiscible basaltic melts than the data from melts at fO_2 = NNO. Power-law equations fitting the data for the hydrous melts are D_P (NNO) = 1.07 $(\text{nbo}/t^f)^{-1.79}$ (r^2 = 0.79) and D_S (NNO, MH) = 4.15$(\text{nbo}/t^f)^{-108}$ (r^2 = 0.72). Partitioning coefficients for melts with F ($D_F = 1 \pm 0.6$), however, do not yield a power-law curve. The addition of plagioclase (An_{50}) to melts in the system Fe_3O_4–$KAlSi_2O_6$–SiO_2 increases the quantities of P, S and F that can be accommodated in the felsic melt.

Application of partitioning–polymerization relationships in experimental melts to the assessment of coexisting, volatile-rich natural magmas

Bogaerts and Schmidt (2006) demonstrated that power-law curves for D_i as a function of nbo/t^f for the elements Fe, Si and Ti in immiscible melts in the basaltic system can be used to discriminate between coexisting melts generated by liquid-phase separation and those resulting from other processes. Major element partitioning data from rocks formed from coexisting immiscible magmas plot either proximal to or as extensions of the power-law curves derived for immiscible melts in the basaltic system. Major element partitioning data from rocks formed from coexisting magmas that were generated by other processes are distinct from those of the immiscible basaltic system. The method has been applied to rocks generated by both intrusive and extrusive coexisting magmas over a wide range of P–*T*–X–fO_2 conditions. A comparison of power-law relationships established for D_i–nbo/t^f relationships for the elements Fe, Si and P in the melts produced in this study with those calculated for the same elements in the basaltic system shows that the power-law equations calculated for the basaltic system can be applied to volatile-rich magmas (Fig. 5) over a wide fO_2 interval, e.g., QFM–MH. Further, the method is applicable even if the H_2O and Fe^{3+} contents of the magmas are not considered in calculating the polymerization parameter nbo/*t*. The finding is non-trivial because quantification of the volatile constituents and Fe^{3+} in igneous rocks and magmas is often problematic.

Immiscibility in volatile-rich magmas

H_2O, P, S, F and Cl are common constituents in most magmatic systems, and understanding their effects on silicate liquid-phase separation constitutes a critical step in the assessment of the role of silicate immiscibility in petrogenesis. Although the melt compositions employed herein are simplified, the documented effects of H_2O, P, S, F and Cl in the experimental systems provide a basis for understanding the potential influence of these constituents in natural magmatic systems.

The effect of H_2O alone or H_2O in combination with P or S is to increase the *T*–*X* range of miscibility gaps in silicate melts (Fig. 5) by suppressing the saturation temperatures of liquidus minerals. F and Cl increase the activity of SiO_2 in the melt, thereby expanding the *T*–*X* stability fields of SiO_2 minerals. The addition of H_2O and F or Cl to the experimental mixtures increases the SiO_2 mineral saturation surface, reducing the compositional extent of the miscibility gap in the F-bearing system and eliminating it altogether in the melts with Cl. Predictably,

the stability fields of SiO_2 minerals and magnetite expand with increasing oxygen fugacity. The phase relations demonstrated here have general implications for the genesis of magnetite deposits of the Kiruna and El Laco type. The origin of these deposits has long been controversial. Sillitoe (2003) and Hitzman et al. (1992) among others propose that these deposits are hydrothermal lithologies, whereas Chen et al. (2010), Naslund et al. (2002) and others invoke liquid-phase separation of immiscible volatile, Fe- and Si-rich magmas as a petrogenetic mechanism. Rocks associated with these deposits are typically enriched with phosphorus and sulfur and have mineralogy and morphology characteristic of H_2O enrichment (Nystroem and Henrique 1994; Naslund et al. 2002).

Melt inclusions in dacite from the El Laco Fe-oxide deposit (Chile), comingled absarokitic basalt and peraluminous monzogranite from the Antauta hypabyssal complex of the Picotani Group (Peru) and Fe-rich spheres in andesitic rock from the Dongargarh Supergroup (India) have been interpreted as having formed from the unmixing of volatile-rich silicate magma (Naslund et al. 2002; Clark and Kontak 2004; Sensarma et al. 2000). Iron partition coefficient (D_{Fe}) and felsic-melt polymerization values (expressed as nbo/t^f) calculated for the coexisting melts in these rocks are distinct from values calculated for coexisting rocks formed by other processes, and they plot above the power-law curves derived for the conjugate liquids produced in this study (Fig. 4a, d).

The expanded *T–X* range of the silicate-liquid miscibility gap and degree of Fe enrichment of the mafic conjugate melts (up to 72 wt% FeO_{total}) produced by the addition of H_2O, P and S to melts in this study, although by no means conclusive, support an immiscible petrogenetic hypothesis for some Fe-oxide deposits. In addition, the reduction in melt viscosity produced by the presence of H_2O favors the efficient separation of conjugate liquids by density, an important component of the immiscible petrogenetic model for the Kiruna ore deposit type.

Implications for the pressure stability of volatile-rich immiscible magmas

The effects of H_2O on the *T–X* configuration of the liquidus surface relative to the miscibility gap in the experimental melt systems have important implications for the pressure stability of two-liquid fields in H_2O-rich natural magmas. To clarify the effects of pressure on liquid-phase separation in H_2O-rich silicate melts, it is useful to consider: (a) the effects of pressure on the mixing parameters in the melts, specifically, on the *T–X* range of the two-liquid field, independent of the liquidus surface configuration; (b) the differences in the effects of pressure on the *T–X* configuration of the liquidus mineral saturation surface between anhydrous and H_2O-rich melts; and (c) the combined effects of (a) and (b) on the *T–X* configuration of two-melt field relative to the liquidus surface and the upper temperature limit of the miscibility gap.

In anhydrous silicate melts, increasing pressure either has little effect or expands the *T–X* extent of two-melt field miscibility gaps (Hudon et al. 2004; Visser and Koster van Groos 1979c; Watson and Naslund 1978), but increasing pressure commonly elevates liquidus surface temperatures above the miscibility gap, with the net effect that two-liquid fields are rarely intersected during the liquid line of descent of most anhydrous or H_2O-poor magmas.

The effect of pressure on two-melt fields in H_2O-rich melts is likely to differ significantly from that in anhydrous systems because the suppression of liquidus temperatures produced by H_2O is nearly independent of pressure up to 2 GPa (Médard and Grove 2008; Almeev et al. 2007; Gaetani and Grove 1998). The extent of stable immiscibility in H_2O-rich melts at pressures commensurate with mid- to deep crust and upper mantle environments is therefore dependent on composition and two competing effects: the increase in anhydrous melt liquidus temperatures as a function of increasing pressure and the magnitude of H_2O-induced liquidus suppression in H_2O-rich melts. For example, in basaltic melts at 2 GPa (fO_2 = NNO), 5 wt% H_2O lowers the olivine liquidus temperature by 137 °C, whereas the dry olivine liquidus temperature is increased as a function of pressure over a 2 GPa range by 130 °C. The net result is that at 2 GPa, the olivine liquidus temperature in H_2O-rich basaltic melts is slightly lower than that of the anhydrous melt at 0.101 MPa, 1,241 °C and 1,248 °C (Médard and Grove 2008). The H_2O-rich experimental melts produced in this study differ from the basaltic system in that they have fewer network- modifying species, and magnetite rather than forsterite is the primary liquidus mineral. Nonetheless, the magnitude of the H_2O-induced liquidus suppression in the experimental melts, although fO_2 dependent, is similar to that of the basaltic system, e.g., ΔT liquidus of the experimental melts, ~120 °C at fO_2 = NNO, ~200° at fO_2 = MH and basaltic melt ~137 °C at fO_2 = NNO.

Considering that liquid miscibility gaps (sensu stricto) in silicate liquids are either independent of or enhanced by increasing pressure and that H_2O-induced suppression of liquidus temperatures is nearly independent of pressure over a wide range of compositions at pressures up to 2 GPa, we infer that the *T–X* configuration of two-liquid fields in H_2O-rich silicate melts at 2 GPa will be similar to that of compositionally equivalent anhydrous melts at low pressures. In addition, although the upper critical temperatures of the miscibility gaps in the experimental systems considered here have not been established, they must be above the experimental upper thermal range (>1,210 °C), in

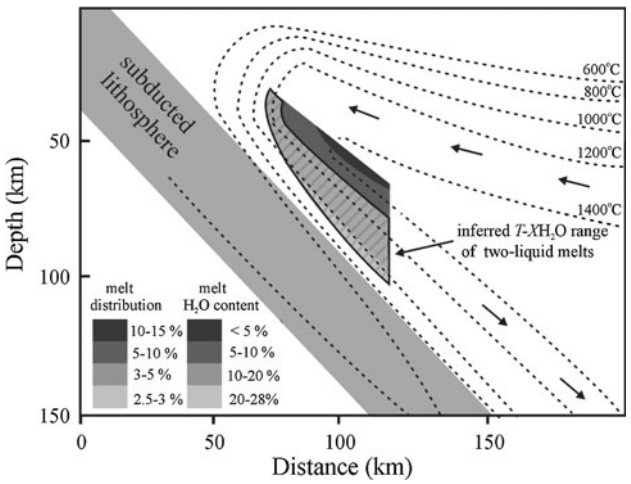

Fig. 6 Inferred T–X H_2O range of two-liquid silicate melts in volatile-flux melting environment (temperature distribution and flux melting processes in the mantle wedge from Grove et al. 2006)

excess of the upper critical temperature of similar anhydrous melts (Fig. 5). The relative increase in upper critical temperature in the hydrous melts is likely to extend further the area of the two-liquid field above the liquidus in H_2O-rich silicate melts.

Water-rich magmas are typically generated in primary melts in subduction zones by volatile-flux melting or in highly evolved magma systems that are enriched with volatile components during the crystal fractionalization process. Magmas in supra-subduction zone environments that contain sufficient H_2O to lower liquidus temperatures enough to stabilize two-liquid fields at depth (≥5 wt%) have been described in experimental and theoretical models of mantle wedge melting (e.g., Grove et al. 2006; Ulmer 2001). The studies delineate an extensive polythermal region within the mantle wedge, where primary, H_2O-rich melts (5–28 wt% H_2O) are generated. The T–X H_2O field that we infer to be permissive of silicate-liquid immiscibility lies within the T–X region where volatile-enriched melts are generated (Fig. 6), suggesting that silicate magma unmixing may be stable in liquids in deep arc environments. The process, though conjectural, describes an interesting mass-flux mechanism which, in conjunction with the contemporaneous mechanical segregation of conjugate melts, could concentrate and transport small but cumulatively significant quantities of Fe and volatile elements in supra-subduction zone environments.

Conclusions

The addition of H_2O alone or in combination with small amounts of P, S or F (1, 2 and 6 wt% oxide totals, respectively) to melts in the systems Fe_2SiO_4–Fe_3O_4–$KAlSi_2O_6$–SiO_2, Fe_3O_4–$KAlSi_2O_6$–SiO_2 and Fe_3O_4–Fe_2O_3–$KAlSi_2O_6$–SiO_2 expands the T–X range of the two-liquid miscibility gap. P and S partition strongly into the mafic melt, whereas F is nearly equally partitioned between the conjugate melts. Liquid-phase separation in melts with H_2O + Cl is restricted to a narrow composition range as the result of the Cl-induced increase in the stability of silica minerals. The addition of 2 wt% S to the system Fe_3O_4–Fe_2O_3–$KAlSi_2O_6$–SiO_2 stabilizes three immiscible melts with Fe-rich mafic silicate, Fe-poor felsic silicate and FeS compositions.

Power-law curves calculated for D_i–nbo/t^f relationships for the elements Fe, Si and P in the melts produced in this study are similar to, but distinct from, those calculated for the same elements in immiscible basaltic melts. The results show that the power-law equations calculated for the basaltic system by Bogaerts and Schmidt (2006) can be applied to assess coexisting volatile-rich magmas over a wide range of P–T–X–fO_2 conditions. Further, the method is applicable even if the H_2O and Fe^{3+} contents of the magmas are not considered in calculating the polymerization parameter nbo/t^f.

Water-induced suppression of liquidus temperatures in the experimental systems, considered with the effects of pressure on the temperature and composition ranges of two-liquid fields in silicate melts, suggests that liquid-phase separation may occur in some H_2O-rich silicate magmas at pressures up to 2GPa. The expanded T–X range of the silicate-liquid miscibility gap and degree of Fe enrichment of the mafic conjugate melts (up to 72 wt% FeO_{total}) produced by the addition of H_2O, P and S to melts in this study add support to the hypothesis that silicate magma unmixing is involved in the genesis of some Fe-oxide deposits.

Acknowledgments Gordon Moore and John Holloway thanked for their assistance in this experimental study. Reviews by Adam Simon and two anonymous reviewers were very helpful and served to significantly improve the manuscript. This research was supported by grants from the Society of Economic Geology and NSERC.

References

Almeev R, Holtz F, Koepke J, Parat F, Botcharnikov RE (2007) The effect of H_2O on olivine crystallization in MORB: experimental calibration at 200 MPa. Am Miner 92:670–674

Bogaerts M, Schmidt MW (2006) Experiments on silicate immiscibility in the system Fe_2SiO_4–$KAlSi_3O_8$–SiO_2–CaO–MgO–TiO_2–P_2O_5. Contrib Miner Petrol 152:257–274

Botcharnikov RE, Almeev RR, Koepke J, Holtz F (2008) Phase relations and liquid lines of descent in hydrous ferrobasalt—implications for the Skaergaard intrusion and Columbia River flood basalts. J Petrol 49(9):1687–1727

Bowen NL (1925) Concerning evidence of immiscibility in a silicate magma, Agate Point Ontario. J Geol 23:629–631

Chen H, Clark AH, Kyser TK, Ullrich TD, Baxter R, Chen Y, Moody TC (2010) Evolution of the Giant Marcona-Mina Justa iron oxide-copper-gold district, South-Central Peru. Econ Geol 105:155–185

Chou IM, Cygan GL (1990) Quantitative redox control and measurement in hydrothermal experiments. In: Spencer RJ, Chou IM (eds) Fluid–mineral interactions: a Tribute to H. P. Eugster, 2. Geochemical Society, Special Publication, pp 3–15

Clark AH, Kontak DJ (2004) Fe-Ti-P oxide melts generated through magma mixing in the Antauta subvolcanic center, Peru: implications for the origin of nelsonite and iron oxide-dominated hydrothermal deposits. Econ Geol 99(2):377–395

Darling RS, Florence FP (1995) Apatite light rare earth element chemistry of the Port Leyden nelsonite, Adirondack Highlands, New York; implications for the origin of nelsonite in anorthosite suite rocks. Econ Geol 90(4):964–968

Dixon S, Rutherford MJ (1979) Plagiogranites as late-stage immiscible liquids in ophiolite and mid-ocean ridge suites: an experimental study. Earth Planet Sci Lett 45:45–60

Dolejs D, Baker DR (2007) Liquidus Equilibria in the system K_2O–Na_2O–Al_2O_3–SiO_2–F_2O_{-1}–H_2O to 100 MPa: II. differentiation paths of fluorosilicic magmas in hydrous systems. J Petrol 48:807–828

Freestone IC, Powel R (1983) The low temperature field of liquid immiscibility in the system K_2O-Al_2O_3-FeO-SiO_2 with special reference to the join fayalite-leucite-silica. Contrib Miner Petrol 82:291–299

Gaetani GA, Grove TL (1998) The influence of water on melting of mantle peridotite. Contrib Miner Petrol 131:323–346

Gaetani GA, Grove T, Bryan WB (1994) Experimental phase relations of basaltic andesite from Hole 839b under hydrous and anhydrous conditions. In: Hawkins JW et al (eds) Proceedings of the Ocean Drilling Program, Scientific Reports, vol 135, pp 557–563

Grove TL, Chatterjee N, Parman SW, Médard E (2006) The influence of H_2O on mantle wedge melting. Earth Planet Sci Lett 249:74–89

Haughton DH, Roeder PL, Skinner BJ (1974) Solubility of sulfur in mafic magmas. Econ Geol 69(4):451–467

Hess PC, Rutherford MJ, Guillmette RN, Ryerson FJ, Tuchfeld HA (1975) Residual products of fractional crystallization of lunar magmas: an experimental study. In: Proceedings of the 6th lunar planet science conference, 1, pp 895–909

Hitzman MW, Oreskes N, Einaudi MT (1992) Geological characteristics and tectonic settings of Proterozoic iron oxide (Cu–U–Au–REE) deposits, in Gaal, G and Schulz, K eds. Precambrian Res 58:241–287

Holloway JR (1971) Internally heated pressure vessels. In: Ulmer GC, Barnes HE (eds) Research techniques for high temperature and pressure. Springer, New York, pp 217–257

Holloway JR, Dixon JE, Pawley AR (1992) An internally heated, rapid-quench, high-pressure vessel. Am Miner 77:643–646

Hudon P, Jung I, Baker DR (2004) Effect of pressure on liquid–liquid miscibility gaps: a case study of the systems CaO–SiO_2, MgO–SiO_2, and $CaMgSi_2O_6$–SiO_2. J Geophys Res 109(B03207):18

Johnson K, Barnes CG, Browning JM, Karlsson HR (2002) Petrology of iron-rich magmatic segregations associated with strongly peraluminous trondhjemite in the Cornucopia stock, northeastern Oregon. Contrib Miner Petrol 142:564–581

Kyser TK, Lesher CE, Walker D (1998) The effects of liquid immiscibility and thermal diffusion on oxygen isotopes in silicate liquids. Contrib Miner Petrol 133:373–381

Laroque A, Stimac J (2000) Evidence for open system behavior in immiscible Fe-S-O liquids in silicate magmas: implications for contribution of metal and sulfur to ore-forming fluids. Can Miner 38:1233–1249

Lester GW (2002) The effects of excess H_2O and H_2O in combination with F, Cl S, or P on liquid immiscibility in the system Si–Fe–Al–K–O at 2 kbar: implications for the genesis of iron-oxide magmas. Unpublished M.A. thesis, State University of New York at Binghamton, p 66

Longhi J (1990) Silicate liquid immiscibility in isothermal crystallization experiments. In: Proceedings of the 20th lunar planetary science conference, pp 13–24

Manning D (1981) The effect of F on liquidus phase relations in the system Qtz–Ab–Or with excess water at 1 kb. Contrib Miner Petrol 76:206–215

McBirney AR (1975) Differentiation of the Skaergaard intrusion. Nature 253:691–694

Médard A, Grove T (2008) The effect of H_2O on the olivine liquidus of basaltic melts: experiments and thermodynamic models. Contrib Miner Petrol 155:417–452

Moore G, Vennemann T, Carmichael ISE (1998) An empirical model for the solubility of H_2O in magmas to 3 kilobars. Am Miner 83:3642

Naldrett AJ (2005) A history of our understanding of magmatic Ni–Cu sulfide deposits. Can Miner 43:2069–2098

Naslund HR (1983) The effect of oxygen fugacity on liquid immiscibility in iron-bearing silicate melts. Am J Sci 283: 1034–1059

Naslund HR, Henríquez F, Nyström JO, Vivallo W, Dobbs FM (2002) Magmatic iron ores and associated mineralisation: examples from the Chilean High Andes and Coastal Cordillera. In: Porter TM (ed) Hydrothermal iron oxide copper-gold & related deposits: a global perspective, 2. PGC Publishing, Adelaide, pp 207–226

Nystroem JO, Henriquez F (1994) Magmatic features of iron ores of the Kiruna type in Chile and Sweden; ore textures and magnetite geochemistry. Econ Geol 89(4):820–839

Philpotts AR (1967) Origin of certain iron–titanium oxide and apatite rocks. Econ Geol 62:303–315

Philpotts AR (1982) Compositions of immiscible liquids in volcanic rocks. Contrib Miner Petrol 80:201–218

Philpotts AR (2008) Comments on: liquid iImmiscibility and the evolution of basaltic magma. J Petrol 49:2171–2175

Philpotts AR, Doyle CD (1983) Effect of magmas oxidation state on the extent of silicate liquid immiscibility in a tholeiitic basalt. Am J Sci 283:967–986

Rajesh HM (2003) Outcrop-scale silicate liquid immiscibility from an alkali syenite (A-type granitoid)-pyroxenite association near Puttetti, Trivandrum Block, South India. Contrib Miner Petrol 145:612–627

Roedder EW (1951) Low temperature liquid immiscibility field in the system K_2O–FeO–Al_2O_3–SiO_2. Am Miner 36:282–286

Roedder EW (1978) Silicate liquid immiscibility in magmas and in the system K_2O–FeO–Al_2O3–SiO_2: an example of serendipity. Geochim Cosmochim Acta 42:1597–1617

Roedder EW, Weiblen PW (1971) Petrology of silicate melt inclusions, Apollo 11 and 12, and terrestrial equivalents. In: Proceedings of the 2nd lunar science conference, pp 507–528

Rutherford MJ, Hess PC, Daniel GH (1974) Experimental liquid line of descent and liquid immiscibility for basalt 70017. In: Proceedings of the 5th lunar science conference, 1, pp 569–583

Ryerson FJ, Hess PC (1978) Implications of liquid–liquid distribution coefficients to mineral-liquid partitioning. Geochim Cosmochim Acta 42:921–932

Ryerson FJ, Hess PC (1980) The role of P_2O_5 in silicate melt. Geochim Cosmochim Acta 44:611–624

Schuessler JA, Roman RE, Botcharnikov E, Behrens H, Misiti V, Freda C (2008) Oxidation state of iron in hydrous phonotephritic melts. Am Miner 93:1493–1504

Sensarma S, Palme H, Deloule E, Mukhopadhyay (2000) Evidence of silicate liquid immiscibility in the early Proterozoic andesitic rock, Dongargarh Supergroup, Central India and possible tectonic implication. Goldschmidt J Conf Abst, 5: 904 Cambridge Publications, Oxford

Sillitoe RH (2003) IOCG deposits: an Andean view. Mineralium Depositum 38:787–812

Visser W, Koster van Groos AF (1979a) Phase relations in the system K_2O-FeO-Al_2O_3-SiO_2 at 1 atmosphere with special emphasis on low temperature liquid immiscibility. Am J Sci 279:70–91

Visser W, Koster van Groos AF (1979b) Effect of P_2O_5 and TiO_2 on liquid–liquid equilibria in the system K_2O-FeO-Al_2O_3-SiO_2. Am J Sci 279:970–988

Visser W, Koster van Groos AF (1979c) Effect of pressure on liquid immiscibility in the system K_2O-FeO-Al_2O_3-SiO_2- P_2O_5. Am J Sci 279:1160–1175

Wallace PJ, Carmichael ISE (1994) S speciation in submarine basaltic glasses as determined by XKα X-ray wavelength shifts. Am Miner 79:161–167

Watson EB (1976a) Two-liquid partition coefficients: experimental data and geochemical implications. Contrib Miner Petrol 56:119–134

Watson EB (1976b) Experimental studies bearing on the nature of silicate melts and their role in trace element geochemistry. Ph.D. Thesis, Massachusetts Institute of Technology, Cambridge

Watson EB, Naslund HR (1978) The effects of pressure on liquid immiscibility in the system K_2O–FeO–Al_2O_3–SiO_2–CO_2. Carnegie Inst Year B 77:410–414

Webster JD, De Vivo B (2002) Experimental and modeled solubilities of chlorine in aluminosilicate melts, consequences of magma evolution, and implications for exsolution of hydrous chloride melt at Mt. Somma-Vesuvius. Am Miner 87:1046–1061

Ulmer P (2001) Partial melting in the mantle wedge and the role of H_2O in the genesis of mantle-derived arc-related magmas. Phys Earth Planet Inter 127:215–232